Radio Science, Volume 36, Number 4, Pages 643–669, July–August 2001

Concepts, observations, and simulation of refractive index turbulence in the lower atmosphere

John C. Wyngaard, Nelson Seaman, Shari J. Kimmel, and Martin Otte
Department of Meteorology, Pennsylvania State University, University Park, Pennsylvania

Xaio Di
Applied Research Laboratory, Pennsylvania State University, University Park, Pennsylvania

Kenneth E. Gilbert
National Center for Physical Acoustics, University of Mississippi, University, Mississippi

Abstract. Advances in computers and in computational techniques now allow the calculation of electromagnetic (EM) wave propagation through simulated refractive index turbulence in the lower atmosphere. Such applications call for instantaneous turbulence fields, not turbulence statistics, the traditional focus of the turbulence community. We clarify their important differences and review what is known about key statistics of refractive index turbulence. We discuss the calculation of EM propagation with a parabolic equation model that uses composite refractive index fields, the larger scales being calculated with a dynamical mesoscale model and the smaller scales being calculated through large-eddy simulation. The locally, instantaneously sharp top of the atmospheric boundary layer can have a profound effect on forward scatter of EM waves. This top appears to be even sharper than is revealed by conventional measurements, particularly in the convective boundary layer.

1. Introduction

Three parallel developments over the past few decades now allow a new approach to the calculation of electromagnetic (EM) wave propagation in environmental flows, one that does not require inventing your own refractive index fields. They are (1) numerical modeling of environmental flows, (2) numerical simulation of turbulence, and (3) parabolic equation models of wave propagation. All three developments were made possible by the advent of large-scale, high-speed digital computers ~30 years ago.

The first development has led to the remarkable reliability of today's numerical predictions of atmospheric phenomena on scales of tens of kilometers to 1000 km [*Dudhia*, 1993; *Hodur*, 1987; *Pielke et al.*, 1992], which meteorologists call the "mesoscale." Today mesoscale modeling is the workhorse of regional meteorology [e.g., *Black*, 1994]. Not only is it used to produce forecasts for several hours to several days ahead and to test hypotheses formed from observations, but it has also provided new insights into atmospheric structure and dynamics. To predict the evolution of meteorological fields in a limited (subglobal) domain, a mesoscale model uses initial conditions describing the specific case with the detail allowed by the observations and model resolution, plus lateral boundary conditions derived from a global model prediction [*Durran*, 1998]. For very fine resolutions (mesh sizes less than 10 km) the mesoscale model generally uses two or more domains of yet finer, "nested" grids [*Zhang et al.*, 1986]. This procedure limits the introduction of errors due to the relatively coarse resolution lateral boundary predictions of the global model and, by reducing the computational requirements, makes real-time, fine-resolution predictions practical.

Figure 1 shows a mesoscale model's 12 hour predictions of potential temperature, water vapor mixing ratio, and modified refractivity M (defined by *Burk and Thompson* [1997]) along a vertical cross section. We used the Pennsylvania State University–National Center for Atmospheric Research mesoscale model (known as MM5) with three nested grids of 36, 12, and 4 km mesh centered over the Persian Gulf. MM5 is similar to the most advanced operational forecast

Paper number 2000RS002380.
0048-6604/01/2000RS002380$11.00

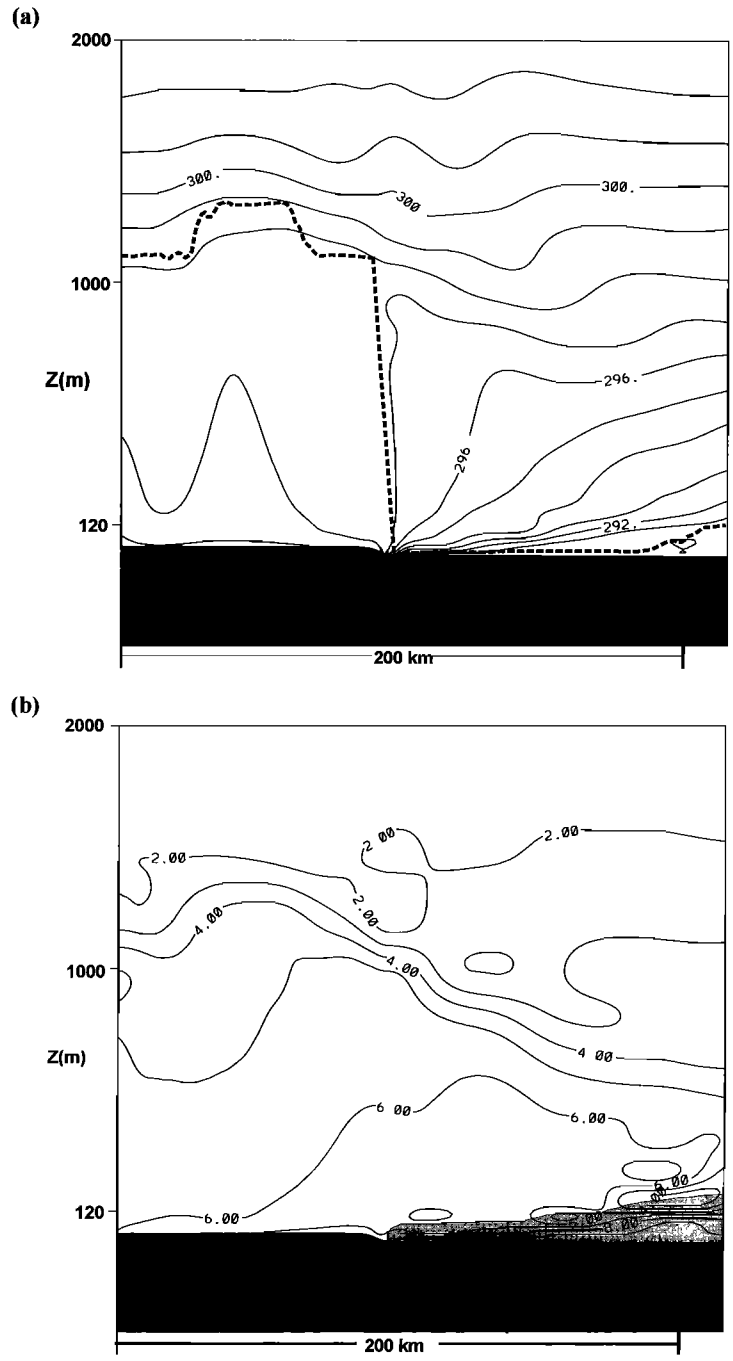

Figure 1. Vertical cross sections over the northwest Persian Gulf showing 12 hour predictions of potential temperature, water vapor mixing ratio, and modified refractivity as a function of height above sea level produced by a 4 km mesh mesoscale model, at 1200 UTC (1500 LST), April 1, 1997. The mean wind flow is northwesterly (left to right in the figure); coastline is approximately 100 km from the left. (a) Isentropes (K) shown as thin solid lines, with thick dashed line representing the height of the convective boundary layer (left) and marine thermal internal boundary layer (right). (b) Contours of water vapor mixing ratio (g kg^{-1}), with shaded area denoting region having a vertical gradient of mixing ratio less than -0.20×10^{-4} g kg^{-1} m^{-1}. (c) Profiles of modified refractivity M along cross-section path at 7 km intervals with shaded areas showing an EM duct capped by a region in which M decreases with height (trapping layer). Dashed line is as in Figure 1a.

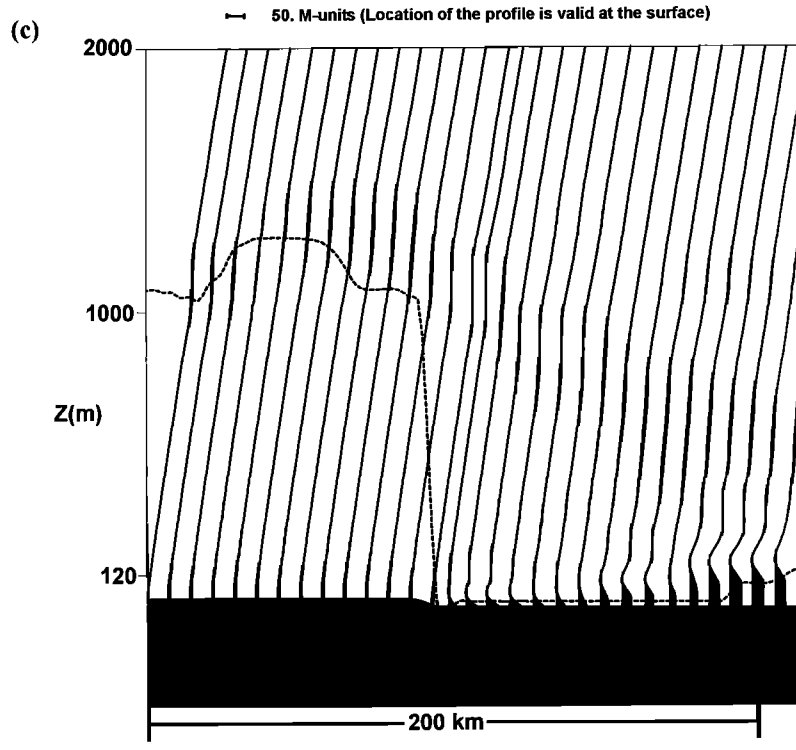

Figure 1. (continued)

models used by National Oceanic and Atmospheric Administration (NOAA) [*Dudhia*, 1993]. Vertical resolution here is 40 m at the surface, gradually increasing with height. The cross section is 200 km in length and oriented northwest-southeast in the northern end of the Persian Gulf [*Seaman and Stauffer*, 1999]. Approximately 80 km of the cross section lie over land (left), and 120 km lie over water (right). The large-scale flow is from the northwest, so the wind is directed offshore; the local time is 1500 LST when the surface temperature and boundary layer depth over land approach their diurnal maxima. In Figure 1a the boundary layer over land is approximately 1200 m deep, while the isentropes show a much shallower, stable internal boundary layer over the cooler sea surface. At the right-hand limit of the figure it has grown to ~150 m in depth. Figure 1b indicates that this shallow marine boundary layer has a strong vertical gradient of moisture, due to intense evaporation from the sea surface into the overlying dry air. The important variations in atmospheric refractivity are controlled primarily by variations in temperature and moisture (section 5), so that the corresponding field of modified refractivity M (Figure 1c) reveals a surface-based EM ducting layer (shaded), capped by a shallow zone where its vertical gradient is negative. This negative M gradient trapping layer is extremely low close to the coastline and gradually rises with distance downwind over the Gulf. Although the vertical resolution of the nearshore structure is limited, the model is capable of predicting the mesoscale structure of individual cases with considerable precision.

According to *Rogallo and Moin* [1984] the numerical solution of the equations governing turbulent flows (known as direct numerical simulation (DNS)), rests largely on foundations laid down by meteorologists at the National Center for Atmospheric Research (NCAR). *Fox and Lilly* [1972] review this earliest work. Because DNS resolves the entire turbulent eddy size range, whose width increases with the flow Reynolds number (section 4), only modest Reynolds number flows can be calculated in this way; they correspond roughly to turbulence in a teacup, say. However, DNS was a breakthrough, the first "no-apologies" turbulence calculation. It gave direct access to the extraordinarily intricate, three-dimen-

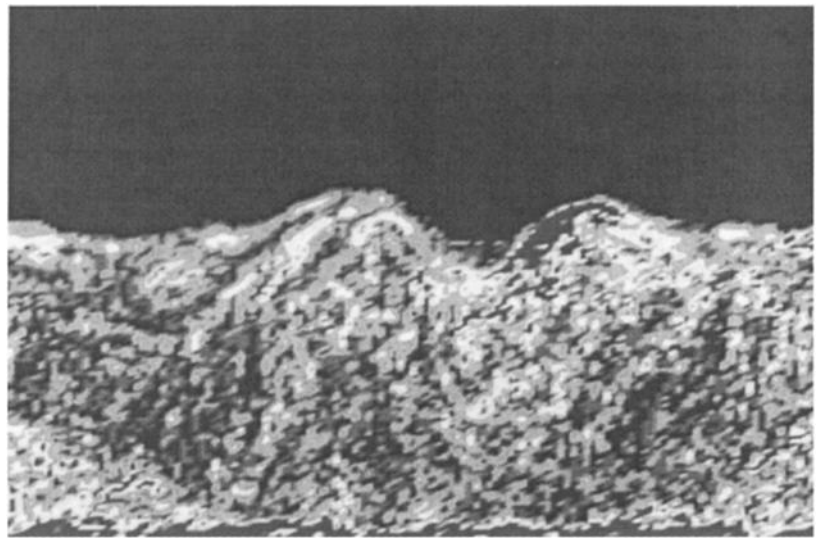

Figure 2. Instantaneous distribution of a conservative tracer ($\nabla q \cdot \omega$, where ∇q is the water vapor mixing ratio and ω is vorticity) in a vertical plane of a convective atmospheric boundary layer (ABL) computed through LES. This tracer is zero in nonturbulent flow and hence reveals the sharp instantaneous top of the convective ABL. The domain is 2.5 km in the horizontal and 1 km in the vertical.

sional, time-dependent, chaotic, nonlinear interactions that are turbulence.

A less pure form of numerical simulation is large-eddy simulation, or LES [*Galperin and Orszag*, 1993]. LES solves (but only approximately) spatially filtered governing equations in which turbulence scales smaller than the filter scale have been removed (section 6). Figure 2 shows a "snapshot" of a vertical plane in a convective atmospheric boundary layer made visible through LES with $\sim 200^3$ grid points in a domain 2.5 km by 2.5 km in the horizontal by 1 km deep. The tracer is the scalar product of vorticity and the gradient of water vapor mixing ratio, a conservative scalar: one whose time rate of change following a fluid element is due only to molecular diffusion. This scalar is a good marker of turbulence, and Figure 2 shows the instantaneously sharp but irregular top of the convective boundary layer and the space-filling nature of the turbulence within it. (As we shall discuss in section 7, it appears that this top is even sharper than LES can resolve.) This is a turbulence simulation counterpart of the acoustic sounding that startled the boundary layer meteorology community in the late 1960s with its graphic displays of the instantaneous atmospheric boundary layer [*McAllister*, 1968].

Much of the original motivation for studying turbulent flows in engineering and in the environment stemmed from what *Taylor* [1935a, 1935b, 1935c, 1935d] called their "virtual mean stresses." These and other virtual fluxes are now better known as Reynolds fluxes after turbulence pioneer O. Reynolds. These ensemble-average (section 4) quantities originate in the random, diffusive movement of constituents by the turbulent velocity field. If the molecular diffusivity of the constituent is on the order of that of momentum, as with temperature and water vapor in air, these Reynolds fluxes exceed the molecular ones by a factor of the turbulence Reynolds number R_t (section 4), which is always large in turbulent flow.

Until a few decades ago we viewed turbulence primarily in the dim light of the ensemble average. The long primacy of ensemble statistics generated through experiment and observation testifies to the impact of the Russian school that included A. N. Kolmogorov. Numerical simulation has fundamentally changed our approach to turbulence, however; today, for better and for worse, the turbulence community is substantially if not predominantly numerical simulation–based.

Parabolic equation (PE) codes allow the direct calculation of EM forward scatter in the lower atmosphere [*Dockery*, 1988; *Kuttler and Dockery*, 1991; *Rogers*, 1998; *Gilbert et al.*, 1999]. Our hard-earned ensemble statistics of turbulence are not obviously

useful here, for the PE technique needs instantaneous refractive index fields, not statistics. It is tempting to "make up" a turbulent refractive index field: through random modes with amplitudes chosen to fit the spectrum of *Obukhov* [1949] and *Corrsin* [1951], for example. However, such a model is apt to be unphysical because it fails to account for the phasing of the Fourier modes that results in spatially coherent eddies and, for example, the instantaneously sharp top of the convective atmospheric boundary layer (section 7). It can also fail to connect turbulence with the larger-scale environment that shapes it.

These three advances, mesoscale meteorological modeling, numerical simulation of turbulence, and the PE technique for calculating wave propagation, make possible a wave propagation solver on the mesoscale (section 7). The mesoscale model can treat the meteorology on scales of 1000 km down to a few kilometers with reasonable accuracy. It cannot resolve the turbulence in the boundary layer, but it can quantify the chief environmental influences on this turbulence. These include the surface heat flux, which generates stabilizing or destabilizing buoyancy forces and dramatically changes the structure of the turbulence; the surface shearing stress, a key scaling parameter for the turbulence generated from wind shear; and the vertical variation of the horizontal pressure gradient that drives the flow, which influences the vertical profiles of the mean wind shear. Knowledge of such parameters allows approximate prediction of the instantaneous refractive index field in the boundary layer through LES (section 7). The linearity of the refractive index conservation equation allows this turbulent fine structure to be added to the mesoscale refractivity fields.

This approach to "wave propagation engineering," as it might be called, is based on instantaneous turbulent refractive index fields. Unfortunately, we do not yet have an agreed-upon set of terms for instantaneous turbulence fields; essentially all of our terms refer to turbulence statistics. The following example illustrates how this can cause problems.

A recent review paper [*Dockery*, 1998] on parabolic equation models for EM propagation in the atmosphere uses the phrase "horizontally homogeneous refractive environments." The refractive environment in the lower atmosphere is usually turbulent, and turbulence is spatially irregular in all three directions, so the phrase could mean "turbulent refractivity of statistically uniform composition in the horizontal"; in turbulence language that is called "horizontally homogeneous turbulence." The author did not explicitly mention turbulence, however, so another possibility is "refractivity that is nonturbulent and uniform in the horizontal."

The author meant the latter (G. D. Dockery, personal communication, 1999). To minimize confusion, we have called this the "plywood approximation" [*Gilbert et al.*, 1999].

Refractive index turbulence has typically been modeled in wave propagation applications. *Hitney* [1993], for example, has included a "troposcatter model" within the PE model called radio physical optics model (RPO) and shows that it can provide improved predictions in some applications. *Hitney* [1993, p. 908] writes, however, "Why this (troposcatter) model works so well is somewhat of a mystery." The resolution of this mystery presumably lies in the still elusive nature of instantaneous refractive index fields.

Adding to the foundations laid by *Gossard and Strauch* [1983] and *Webb* [1984], we shall discuss the underlying concepts of refractive index turbulence in the lower atmosphere, observations of its structure, and its coupling to the larger-scale meteorology. We stress the differences between statistical and instantaneous properties. Since those pieces were written, much has been learned about refractive index turbulence and the wave propagation problem, and the numerical simulation of turbulence has seen explosive growth. Thus we include a discussion of numerical simulation in the context of the EM propagation problem.

Some of the material in this paper is given by *Wyngaard* [1992]. Where possible, we reference journal papers reprinted in the volume edited by *Andreas* [1990].

2. Atmospheric Boundary Layer

"Boundary layer" is an engineering term for the moving fluid layer adjacent to a body. The study of boundary layers was motivated by the conflict between the zero-drag predictions of inviscid fluid mechanics and the observation that a body in a moving fluid does experience drag. Researchers discovered that there is a thin layer near the body within which the flow velocity smoothly transitions from the value at the body surface to the free-stream value. The resulting velocity gradient at the surface generates viscous drag.

Our perceptions about the atmospheric boundary

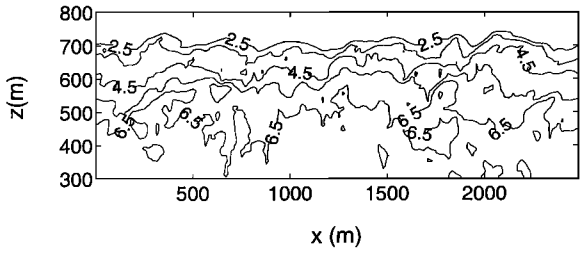

Figure 3. Instantaneous water vapor mixing ratio contours (in g kg^{-1}) in a vertical plane of a convective ABL computed through LES. Near the convoluted boundary between turbulent flow below and nonturbulent flow above, the vertical gradient of mixing ratio can be locally large.

layer (ABL) sharpened when it was made "visible" by acoustic sounders in the late 1960s. Over the ABL depth there can be strong changes in velocity, temperature, and the concentration of water vapor and other trace constituents. Some of the important features of the ABL are as follows:

1. It has continuous, three-dimensional turbulence bounded by a top that is quite different instantaneously and in the ensemble average. The instantaneous top of the convective boundary layer is the thin, convoluted, ever-changing boundary between the turbulent flow and the stably stratified, warmer, drier, nonturbulent flow above (Figure 3). Ensemble, temporal, or spatial averaging produces a transition zone called the "interfacial layer" (Figure 4).

2. Buoyancy is a dominant influence on the ABL and its turbulence. The canonical convective (positive surface heat flux; Figure 5) and stable (negative surface heat flux; Figure 6) ABLs are strikingly different in their structure. The nocturnal boundary layer over land is typically stably stratified through

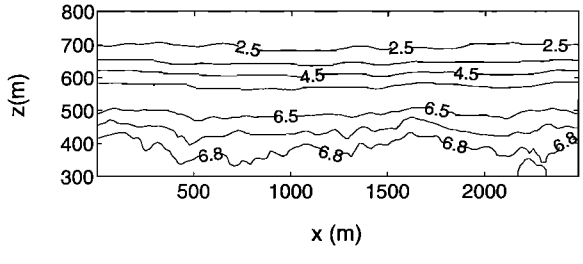

Figure 4. The contours of Figure 3 averaged over the homogeneous y direction and over several times under stationary conditions to approximate an ensemble average. The averaging produces an interfacial layer between turbulent and nonturbulent flow that is smoother and more diffuse than the instantaneous boundary of Figure 3.

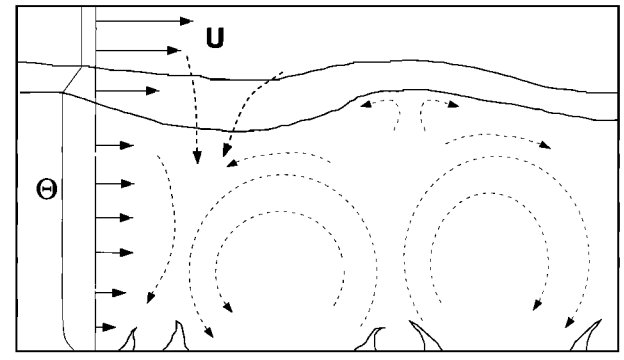

Figure 5. An artist's sketch of a canonical convective ABL showing the large, buoyancy-driven convective eddies and the thin buffer region between the turbulent and nonturbulent fluid. U, mean wind speed; Θ, mean potential temperature.

surface cooling; at some height this extinguishes the turbulence and thereby determines the boundary layer top. The neutral (negligible surface heat flux) ABL is actually quite rare because even small temperature differences generate heat fluxes large enough to cause significant buoyancy effects. When it is found, it is apt to be capped by an inversion.

3. The horizontal wind flow in the ABL is typically driven by a hydrostatically determined horizontal pressure gradient. Horizontal temperature gradients can cause this pressure gradient to vary with height, making its horizontal mean momentum balance more complicated than that of its laboratory counterpart, the boundary layer over a flat plate.

4. The mean ABL depth h can range from tens of meters to a few kilometers. Over land it typically

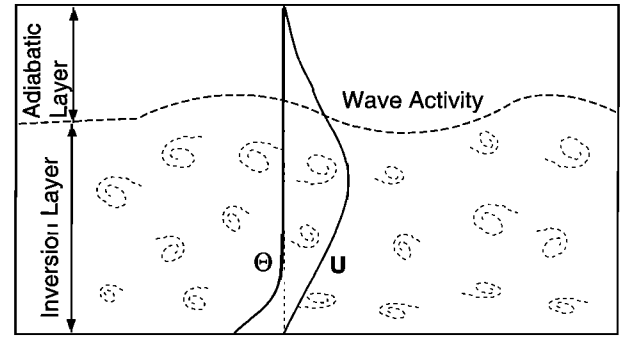

Figure 6. An artist's sketch of a canonical stable ABL. It is characterized by a cooled surface, shear-driven turbulence with eddy size limited by the stable stratification, gravity wave activity, and a maximum in the mean velocity profile. It is usually shallower than a convective ABL.

evolves over the course of the day because of the changing surface energy budget. In clear weather the depth increases with time after sunrise as surface heating drives turbulent convection. In a horizontally homogeneous environment the rate equation for h is

$$dh/dt = w_e + W(h), \quad (1)$$

where w_e is the entrainment velocity due to turbulent entrainment of the overlying inversion and $W(h)$ is the mean vertical velocity at the ABL top. W and w_e are typically on the same order of magnitude. Under high pressure a negative value of W is induced through the interaction of surface friction and Coriolis effects known as "Ekman pumping," and so dh/dt is less than w_e; this tends to limit h and inhibit cloud formation. Mean ABL depth h typically reaches a peak in the afternoon; in late afternoon the surface heat flux vanishes, shutting off the buoyant production of turbulence so the ABL turbulence intensity decays. At night, a thinner, stably stratified boundary layer with shear-driven turbulence develops at the surface and deepens with time.

5. The near-surface portion of the boundary layer, the lowest 10%, say, is called the "surface layer." Because of its accessibility to measurement, it is relatively well understood. Monin-Obukhov similarity describes major aspects of the statistical structure of the surface layer under a wide range of stability conditions, both unstable and stable.

6. The required averaging times for convergence of time-averaged ABL flow statistics to the ensemble averages can be quite large, often larger than the times over which the flow can be considered quasi-steady. For this reason the scatter in atmospheric turbulence measurements tends to be much larger than in engineering flows.

7. Air masses residing over large bodies of water for several days (in the absence of large gradients in sea surface temperature) typically have boundary layer temperatures that differ little from that of the underlying water. Surface heat fluxes in this case tend to be much smaller than over land and do not exhibit strong diurnal dependency.

The monographs by *Stull* [1988] and *Kaimal and Finnigan* [1994] cover the ABL in detail.

3. Turbulence

Turbulence is the random, irregular motion of a moving fluid. Two-dimensional turbulence is dynamically quite different from the ubiquitous three-dimensional variety [*Tennekes*, 1978]; it is a useful model of the general circulation of the atmosphere, whose thickness is small compared to the Earth's diameter. "Random" means different in every realization of the flow; it does not imply that turbulence is Gaussian or of any other specific statistical nature. (Only the even moments of the energy-containing (larger-scale) turbulence are approximately Gaussian.) A turbulent flow of a given geometry with infinitesimally different initial and boundary conditions will evolve differently in every realization of the flow.

Transition from laminar to turbulent flow normally occurs when a Reynolds number UL/ν exceeds a threshold value; here U and L are representative velocity and length scales of the flow, and ν is the kinematic viscosity (dynamic viscosity/density) of the fluid, liquid, or gas. Transition occurs through the instability of the laminar fluid velocity field to perturbations. The spatially and temporally chaotic velocity fluctuations that result from this instability are sufficiently large that they interact through the nonlinear term in the momentum equation; they can keep the turbulent motion in energetic equilibrium by extracting energy from the mean flow.

The randomness of turbulence (the inevitable differences between any two realizations of a turbulent flow) is believed to stem from its sensitive dependence on initial conditions. We can never avoid the small variations in initial conditions that cause each realization of a turbulent flow to be different.

Three-dimensional turbulence owes its ubiquity to the tendency of fluids in motion to become turbulent and the tendency of turbulence to become three dimensional. It occurs in nearly all engineering flows, is found intermittently on smaller scales in the free atmosphere, where it is called "clear-air turbulence," and occurs continuously in clouds, in the atmospheric boundary layer, and in the upper ocean.

Nobel laureate R. Feynman reportedly called turbulence "the last great unsolved problem of classical physics." It remains unsolved. Early workers referred to the "turbulence problem," which meant predicting the Reynolds fluxes so the mean velocity and temperature fields could be calculated. Today we have many more applications for turbulence knowledge, and so the "turbulence problem" has a broader meaning. Today it means calculating the structure of a turbulent flow of arbitrary Reynolds number to a given accuracy. We still have no way to do that.

L. da Vinci was referring to turbulence when he

wrote "Remember, when discoursing about water, to induce first experience, then reason." His advice remains valid today: The study of turbulence proceeds best when it proceeds from observations. Making archival-quality observations of turbulence, particularly in the atmosphere, is very difficult, however, and there has been increasing interest in calculation methods for turbulent flows.

In a review of a monograph on turbulent diffusion, *Scorer* [1980, p. 148] wrote "... because turbulence makes itself more complicated all the time so that no full description is possible, most theories are not theories about the turbulence at all, but about the consequences.... In the great outdoors we have, particularly in the atmosphere, an unending succession of different cases, whereas it is a characteristic of the models that they refer only to particular cases. One is always bound to wonder whether the models are relevant enough to be worth the bother...." *Hunt* [1981, p. 126] responded, "This approach is dismissed as useless by Professor Scorer... because nature is too complicated, he says, it cannot be codified... if we are to follow his advice and discuss nature eddy by eddy, how is the government [air-quality] inspector to make his decision and how are others to argue with him?"

This exchange hints not only at the controversy that has attended the modeling of atmospheric turbulence but also at one of the important features of turbulence: its large excursions about an ensemble-mean state. *Scorer*'s [1980] lament is particularly relevant to modeling EM propagation through parabolic equation techniques. With the new turbulence modeling approaches (section 7) one can hope to represent the atmosphere's "unending succession of different cases."

4. Describing and Representing Turbulence

4.1. Statistical Properties and Individual Realizations

Most of the descriptive terms for turbulence refer to its statistical properties, the traditional focus of turbulence research. These terms can be confusing to the nonspecialist. For example, in everyday usage, "homogeneous" means "of uniform structure and composition throughout." Thus "homogeneous turbulence" might seem incongruous. It is not; it means turbulence whose statistics are independent of position. Likewise, "steady" or "stationary" turbulence has statistics that are independent of time. "Isotropic turbulence" is statistically independent of translation, rotation, and reflection of the coordinate axes. The logarithmic wind profile (the proportionality of the mean wind speed to the logarithm of distance z from the surface) and the constant-flux layer (the near constancy of turbulent fluxes with z near the surface) are statistical properties of the flow near the Earth's surface; they exist only on average, not instantaneously.

Today we can produce instantaneous turbulence fields from remote sensors and from numerical solution of the fluid equations, but unfortunately, we do not yet have nomenclature for them. We might be tempted to describe their spatial character as "inhomogeneous" and their time behavior as "unsteady," for example, but we dare not, for those terms describe statistical properties.

4.2. Ensemble Averaging

In turbulence all the flow properties (velocity, pressure, temperature, water vapor density, and refractive index) are distributed irregularly in space, fluctuate chaotically in time, tend to be correlated with each other, and are different in every realization. Following *Tennekes and Lumley* [1972], we use tildes to signify these turbulent dependent variables. In many applications we need only their mean values, and so it has been traditional to separate every flow property $\tilde{a}(x_i, t)$ into mean and fluctuating parts,

$$\tilde{a}(x_i, t) = \bar{\tilde{a}}(x_i, t) + a'(x_i, t) = A(x_i, t) + a(x_i, t), \qquad (2)$$

where $\bar{\tilde{a}}$ or A is the mean and a' or a is the fluctuation. Both the overbar-prime and uppercase-lowercase conventions are used in the literature. We will use the uppercase and lowercase convention where possible.

One can use several types of averages to define mean values in turbulence. A time average is useful when the flow is statistically steady, which is not always the case. The earliest papers in turbulence [e.g., *Reynolds*, 1895] used a volume average. In numerical modeling we often use a volume or area average to remove smaller-scale information. The Russian school introduced the ensemble average: the limit of the average over realizations of a flow as the number of realizations goes to infinity. It is discussed by *Batchelor* [1960] and *Lumley and Panofsky* [1964].

The ensemble average has ideal properties: It is linear, it commutes with differentiation, and succes-

sive applications have no further effect. Formal statistical treatments of turbulence generally use it. It can be impractical with typical observations, however.

We can illustrate the ensemble average with a laboratory turbulent flow driven by a blower. A flow property $\tilde{a}(\mathbf{x}, t)$, where $\mathbf{x}$ is position and t is time (measured from the instant the flow is initiated, say), is a random variable, different in every realization. Every time history of $\tilde{a}$ measured at a given position in the flow will be different and every "snapshot" of the spatial field of $\tilde{a}$ at a given time will be different. We can indicate this randomness by writing the property as $\tilde{a}(x_i, t; \alpha)$, α denoting the realization number.

The ensemble average of $\tilde{a}$ is defined by

$$\bar{\tilde{a}}(x_i, t) = A(x_i, t) \equiv \lim_{N\to\infty} \frac{1}{N} \sum_{\alpha=1}^{N} \tilde{a}(x_i, t; \alpha). \qquad (3)$$

Because it holds both position and time fixed, the ensemble average allows a mean value to depend on both position and time.

A time average is almost always used with turbulence observations. Some combine spatial averaging (e.g., along aircraft flight paths) with time averaging and averaging over runs made under the same general conditions. In numerical simulation we often use spatial, temporal, and ensemble averaging.

By the ergodic hypothesis [*Tennekes and Lumley*, 1972] a time average under stationary conditions and a spatial average in a homogeneous direction converge to the ensemble average. The theory of this convergence is well established [*Lumley and Panofsky*, 1964; *Tennekes and Lumley*, 1972]. For a time series the required averaging time (measured in integral scales) for determining the mean of a stationary time series to a given "uncertainty" (the rms difference between the time and ensemble means divided by the ensemble mean) varies directly as the ratio of the variance and the squared mean of the signal, and inversely as the square of the desired uncertainty.

The 1968 Kansas surface layer experiment showed that the required averaging times for turbulence statistics in the ABL can be surprisingly long; for example, the constant-flux layer near the surface emerged only after several tens of hours of flux data were averaged [*Haugen et al.*, 1971]. Some statistics converge even more slowly than others; stress requires much longer averaging time than variances, for example. Obtaining stresses in a convective ABL at a height of 200 m that are as good, scatterwise, as 1 hour stresses measured at 10 m, say, requires an averaging time of ~50 hours [*Wyngaard*, 1973]. Long averaging times are not the answer because they can seldom exceed a few hours before nonstationarity effects creep in.

Obtaining low-scatter data from midregions of the convective boundary layer, data averaged sufficiently long to minimize its scatter, is a formidable problem.

4.3. Spatial Filtering

Turbulent velocity fields have a wide range of spatial scales. Most of the kinetic energy is associated with fluctuations, or eddies, of spatial scale l which is on the order of the flow scale. These are called the "energy-containing" eddies. *Kolmogorov* [1941] hypothesized that the length scale of the smallest, "dissipative" eddies is on the order of $\eta = (\varepsilon/\nu)^{1/4}$, where ε is the rate of molecular destruction of turbulence kinetic energy per unit mass and ν is the kinematic viscosity of the fluid. Length scale η is now called the Kolmogorov microscale. Measurements in a wide variety of turbulent flows show that $\varepsilon \simeq u^3/l$, where u is the characteristic velocity of the energy-containing eddies. It follows that the eddy size range in any (three-dimensional) turbulent flow is

$$\frac{\ell}{\eta} = \frac{\ell}{(\nu^3/\varepsilon)^{1/4}} \simeq \left(\frac{u\ell}{\nu}\right)^{3/4} = R_l^{3/4}, \qquad (4)$$

R_l being a Reynolds number of the energy-containing eddies. Resolving the dissipative eddies in a direct numerical simulation of turbulence is essential, for they keep the kinetic energy of the flow from growing without limit.

In a daytime ABL the turbulence Reynolds number R_l can be as large as 10^8, so that $l/\eta \simeq 10^6$. Typical values are $l \simeq 10^3$ m, $\eta \simeq 10^{-3}$ m. This scale range is far larger than can be used in the direct numerical solution of the governing equations of fluid motion (DNS). Computer size and speed currently limit DNS to l/η values of a few hundred and R_l values of a few thousand, far smaller than in the ABL.

Nonetheless, DNS can give useful insights into geophysical turbulent flows because the larger-scale structure of turbulent flows can be essentially independent of R_l, provided that R_l exceeds a threshold value. This is called "Reynolds number similarity," a misnomer; it means Reynolds number independence. This threshold value is often within reach of DNS, and DNS is being used today to provide insights into the structure of real turbulent flows in engineering and in geophysics.

In high-R_t flows the only viable approach at present is to spatially filter the equations to remove turbulent detail smaller than a certain scale. Solving these filtered equations numerically requires a spatial mesh size of the order of the filter scale, which can be far larger than the turbulence microscale. We tend to use as many grid points as our computers allow, so we typically choose the filter scale to be as fine as possible, on the order of 1/100 of the domain scale.

Because of the nonlinearity of the flow equations this spatial filtering introduces new terms into the equations, terms that represent the interaction of the resolvable-scale fields with the subgrid-scale fields removed by the filter. These new terms are dynamically essential; for example, in LES they represent the mechanism by which kinetic energy is transferred from resolvable-scale motions to subgrid-scale motions and, ultimately, to the smallest eddies where it is converted to internal energy by viscous dissipation. In practice we cannot represent these subgrid-scale effects in the resolvable-scale equations exactly; we use an approximate subgrid-scale model for this purpose.

The resolvable-scale fields resulting from spatial filtering are not to be confused with ensemble-average fields. Resolvable-scale fields retain some randomness, the amount depending on the scale of the filter. At one extreme, mesoscale modeling, the filter scale is on the order of kilometers in the horizontal. These resolvable-scale fields have very little of the chaotic spatial and temporal variability that we call turbulence; they are more like two-dimensional turbulence. At the other extreme, large-eddy simulation (section 6), the filter scale is small compared to the energy-containing eddies, and the resolvable-scale fields are unmistakably three-dimensionally turbulent.

5. Turbulent Refractive Index Statistics

5.1. Fluctuating EM Refractive Index

The refractive index $\tilde{n} \equiv c_0/\tilde{c}$ for radio waves is given by [*Wesely*, 1976]

$$\tilde{n} - 1 = A\frac{(\tilde{p} - \tilde{e})}{\tilde{T}} + \frac{\tilde{e}}{\tilde{T}}\left(B + \frac{C}{\tilde{T}}\right). \tag{5}$$

Here $\tilde{p}$ is ambient pressure, $\tilde{e}$ is the partial pressure of water vapor, $\tilde{T}$ is ambient temperature, $A = 77.6 \times 10^{-6}$ K hPa^{-1}, $B = 72 \times 10^{-6}$ K hPa^{-1}, and $C = 0.375$ K^2 hPa^{-1}.

Wesely [1976] shows further that if each dependent variable is written as the sum of an ensemble mean and a fluctuation,

$$\tilde{n} = N + n, \quad \tilde{p} = P + p, \quad \tilde{e} = E + e, \quad \tilde{T} = T + \theta, \tag{6}$$

then to a good approximation, the fluctuations are related by

$$n = \left(\frac{A}{T}\right)\left(p - e - P\frac{\theta}{T}\right) + \left(\frac{B}{T} + \frac{C}{T^2}\right)\left(e - E\frac{\theta}{T}\right). \tag{7}$$

Within the boundary layer, ambient pressure fluctuations p can typically be neglected in comparison with water vapor pressure fluctuations e. Thus we can write this in the much simpler form

$$n = a\theta + bq, \tag{8}$$

where q is water vapor mixing ratio and the constants a and b depend on the mean values of pressure, temperature, and water vapor mixing ratio. For radio waves the effect of water vapor fluctuations on n greatly exceeds that of temperature, so we can evaluate the temperature coefficient a for a dry atmosphere. This gives, finally,

$$n = 8.6 \times 10^{-7}(\theta - 7.8q) \tag{9}$$

5.2. Power Spectral Density

The classical representation of turbulence statistics (that of *Batchelor* [1960], for example) uses the ensemble-mean and three-dimensional, homogeneous turbulence fields. The autocorrelation, spectral density transform pair for the fluctuating refractive index n is

$$\phi(\kappa_i, t) = \frac{1}{(2\pi)^3}\int\int\int_{-\infty}^{+\infty} e^{-i\kappa_i r_i}\overline{n^2}R(r_i, t)\, dr_1\, dr_2\, dr_3,$$

$$\overline{n^2}R(r_i, t) = \int\int\int_{-\infty}^{+\infty} e^{i\kappa_i r_i}\phi(\kappa_i, t)\, d\kappa_1\, d\kappa_2\, d\kappa_3, \tag{10}$$

with k_i and r_i being the wave number and spatial separation vectors, respectively, and with the normalized autocorrelation function $R(r_i, t)$ defined as

$$\overline{n^2}R(r_i, t) = \overline{n(x_i, t)n(x_i + r_i, t)}. \tag{11}$$

The overbar represents the ensemble mean. The ensemble-averaging operator allows statistics to depend on time, but we will not generally indicate this explicitly. The spectral density integrates over its

three-dimensional wave number argument to the variance,

$$\int\int\int_{-\infty}^{+\infty} \phi(\kappa_l)\, d\kappa_1\, d\kappa_2\, d\kappa_3 = \overline{n^2}. \qquad (12)$$

It is usual to define a three-dimensional spectrum E_s that is the integral of ϕ over a spherical shell of radius $\kappa = |\kappa_l|$:

$$E_s(\kappa) = \oiint \phi(\kappa_l)\, d\sigma, \qquad \kappa = |\kappa_l|. \qquad (13)$$

Fourier analysis of in situ observations is traditionally carried out in time. The Taylor or frozen-field approximation $\kappa_1 = 2\pi f/U$, with U being the mean wind (or aircraft) speed, is then used to convert the cyclic frequency f to streamwise wave number κ_1. The resulting one-dimensional spectrum is defined through

$$\Phi(\kappa_1) = \frac{1}{2\pi}\int_{-\infty}^{+\infty} e^{-\imath\kappa_1 r_1}\, \overline{n^2} R(r_1, 0, 0)\, dr_1, \qquad (14)$$

the one-dimensional Fourier transform of the autocorrelation function with separation in the streamwise direction. That autocorrelation function is the one-dimensional transform of Φ:

$$\overline{n^2} R(r_1, 0, 0) = \int_{-\infty}^{+\infty} e^{\imath\kappa_1 r_1}\Phi(\kappa_1)\, d\kappa_1. \qquad (15)$$

Because of the aliasing associated with the integration over wave number, the one-dimensional spectrum is not a reliable indicator of spatial scales [*Tennekes and Lumley*, 1972].

The ABL is inhomogeneous in the vertical, so this traditional representation should be applied only to the horizontal directions. The autocorrelation, spectral density transform pair is then

$$\phi_2(\kappa_1, \kappa_2; z) = \frac{1}{(2\pi)^2}\int\int_{-\infty}^{+\infty} e^{-\imath\kappa_i r_i}\, \overline{n^2} R_2(r_1, r_2; z)\, dr_1\, dr_2, \qquad (16)$$

$$\overline{n^2} R_2(r_1, r_2; z) = \int\int_{-\infty}^{+\infty} e^{\imath\kappa_i r_i}\phi_2(\kappa_1, \kappa_2; z)\, d\kappa_1\, d\kappa_2,$$

with the autocorrelation function in the plane defined as

$$\overline{n^2}(z) R_2(r_1, r_2; z) = \overline{n(x_1, x_2, z) n(x_1 + r_1, x_2 + r_2, z)}. \qquad (17)$$

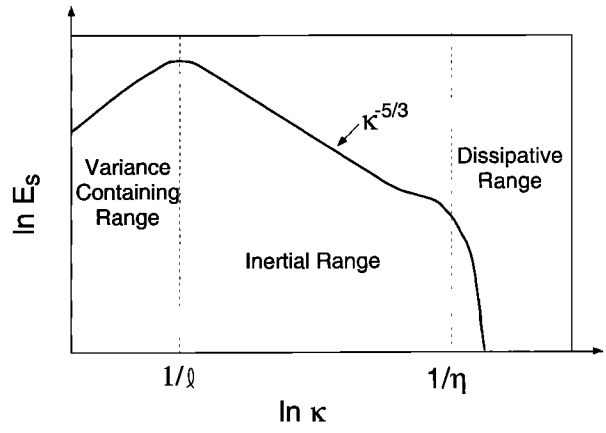

Figure 7. A schematic of the three-dimensional spectrum of a conservative scalar.

The corresponding one-dimensional spectrum in the κ_1 direction, for example, is

$$\Phi_2(\kappa_1) = \int_{-\infty}^{\infty} \phi_2(\kappa_1, \kappa_2)\, d\kappa_2. \qquad (18)$$

In a three-dimensionally homogeneous flow the relation between ϕ_2 and ϕ is

$$\phi_2(\kappa_1, \kappa_2) = \int_{-\infty}^{+\infty} \phi(\kappa_1, \kappa_2, \kappa_3)\, d\kappa_3. \qquad (19)$$

Thus the one-dimensional spectra are the same:

$$\Phi_2(\kappa_1) = \int_{-\infty}^{\infty} \phi_2(\kappa_1, \kappa_2)\, d\kappa_2$$

$$= \int_{-\infty}^{\infty}\int_{-\infty}^{\infty} \phi(\kappa_1, \kappa_2, \kappa_3)\, d\kappa_2\, d\kappa_3 = \Phi(\kappa_1). \qquad (20)$$

The spectrum of refractive index, or of any conservative scalar, has three wave number ranges: the variance-containing range, the inertial range, and the molecular destruction or dissipative range (Figure 7). The first two are generally important in EM propagation. These ranges are defined relative to the scales l and η of the variance-containing and dissipative eddies (this use of the Kolmogorov microscale η assumes that the molecular diffusivity D of the scalar and the kinematic viscosity of air v are equal):

Variance-containing range

$$\kappa = O(\ell^{-1}),$$

Inertial range

$$\ell^{-1} << \kappa << \eta^{-1},$$

Dissipative range

$$\kappa = O(\eta^{-1}).$$

In the turbulence community, l and η have different names in the Western literature and in the Russian literature. The West knows them as the "integral scale" and "Kolmogorov microscale", respectively, while in the Russian literature they are called "outer" and "inner" scales. The EM propagation literature [e.g., *Strohbehn*, 1968] tends to use the Russian names.

At ~300 K, for temperature in air, ν/D (the Prandtl number) is 0.72, and for water vapor in air the corresponding ratio (the Schmidt number) is 0.63. This requires a slight adjustment of the microscale of the temperature and water vapor spectra in air [*Hill*, 1978a].

5.2.1. Variance-containing range. Generally speaking, only the one-dimensional spectrum in the mean wind direction has been measured in the atmospheric boundary layer. It integrates over its argument to the variance,

$$\int_{-\infty}^{\infty} \Phi(\kappa_1)\, d\kappa_1 = \overline{n^2}, \tag{21}$$

although several other conventions are used: combinations of integrating to the half-variance rather than the variance and from 0 to ∞ rather than from $-\infty$ to ∞.

The assumption of isotropy is poor in the variance-containing range; it is dynamically impossible for turbulence to be isotropic at those scales [*Tennekes and Lumley*, 1972].

5.2.2. Inertial range. Isotropy is a standard assumption in the inertial and dissipative ranges, although it is probably not always a good assumption [*Sreenivasan*, 1991]. Under this "local isotropy," as it is called, ϕ depends only on κ. Thus the three-dimensional spectrum is simply

$$E_s(\kappa) = 4\pi\kappa^2\phi(\kappa). \tag{22}$$

The *Obukhov* [1949] and *Corrsin* [1951] form of the three-dimensional spectrum of a conservative scalar in the inertial subrange is

$$E_s(\kappa) = \beta\varepsilon^{-1/3}\chi\kappa^{-5/3}, \tag{23}$$

where $\beta \sim 0.6$ is a universal constant, ε is the rate of viscous dissipation of turbulence kinetic energy per unit mass, and χ is the rate of molecular destruction of scalar variance. In the inertial range the corresponding one-dimensional spectrum is

$$\Phi(\kappa_1) = \tfrac{3}{5}\beta\varepsilon^{-1/3}\chi\kappa^{-5/3} = \beta_1\varepsilon^{-1/3}\chi\kappa^{-5/3}, \tag{24}$$

where β_1 is the one-dimensional spectral constant. Experimentalists usually use a one-dimensional spectrum that integrates over the half line to the variance (rather than over the full line as in (21)), and in the half-line convention, $\beta_1 \simeq 0.4$ [*Champagne et al.*, 1977].

Hill [1978b] has argued that there is a "bump" in the scalar spectrum at the small-scale end of the inertial range (Figure 7), and observations [e.g., *Champagne et al.*, 1977] support this.

5.3. Variances and Covariances

Turbulence tends to make all fluctuating fields correlated in the variance-containing range unless flow symmetry dictates otherwise. Thus, in general, θ and q are correlated, and each is correlated with the fluctuating velocity u_i to produce turbulent fluxes of temperature $\overline{\theta u_i}$ and water vapor $\overline{q u_i}$. These fluxes generally have both vertical and horizontal components, the latter a joint effect of the vertical gradients of mean horizontal wind and the mean scalar [*Wyngaard et al.*, 1971a].

Because of the decrease of pressure with height, the temperature of a vertically displaced air parcel changes, even in the absence of heat transfer. This makes temperature a nonconservative variable in ABL-scale motions. The conservative temperature is the potential temperature $\theta = T(1000/P)^{R/c_p}$, where P is pressure in millibars.

5.3.1. Surface layer. In the surface layer the lowest portion (10%, say) of the ABL (Figure 8), the horizontal components of turbulent scalar fluxes are unimportant, and the vertical components are little changed from their surface values. Being the portion of the atmosphere most accessible to measurement, the surface layer is also the best understood. The Monin-Obukhov similarity hypothesis holds that over a statistically homogeneous surface, at heights above the molecular sublayer but within the "constant-flux" layer (below h_0 in Figure 8), the statistical structure of the energy-containing turbulence depends only on distance z from the surface, the Boussinesq buoyancy parameter $\beta = g/T_0$, the surface temperature flux

Q_0 (the surface heat flux divided by ρc_p, with ρ being the air density and c_p being the specific heat at constant pressure), and the friction velocity (the square root of the kinematic surface stress) u_*. Statistics made dimensionless with scales z (length), u_* (velocity), and $T_* = -Q_0/u_*$ (temperature) are hypothesized to be universal functions of the stability parameter z/L, where $L = -u_*^3/k\beta Q_0$ is the Monin-Obukhov length. (The von Karman constant $k \simeq 0.4$ is traditionally included.) A negative value of z/L is associated with positive Q_0 (upward surface heat flux); this occurs when the surface is warmer than the air and gives thermally unstable conditions.

Both water vapor and temperature can contribute to buoyancy, and this is usually accommodated through the use of virtual temperature $T_v = T(1 + 0.61\, m)$, where m is the specific humidity (essentially equal to the water vapor mixing ratio, mass of water vapor per mass of air). In general, the similarity scales, and expressions are interpreted in terms of virtual temperature.

For large instabilities (negative z/L values of the order of 1) some surface layer statistics show signs of following the predictions of free convection theory, despite the presence of mean wind shear. *Tennekes* [1970] coined the term "local free convection" to describe this regime at the outer edge of the unstable surface layer. It can be interpreted physically as the result of the increasing influence of turbulent buoyancy forces with height; at some height the convective turbulence so dominates the mechanical turbulence that u_* drops out of the governing parameter group. If so, the scales become $u_f = (\beta Q_0 z)^{1/3}$ for velocity, $T_f = Q_0/u_f$ for temperature, and z for length; the local turbulent Richardson number $\beta T_f z/u_f^2$ is then independent of z. In the local free convection limit we expect $\overline{u_3^2} \sim u_f^2$, $\overline{\theta^2} \sim T_f^2$, or, equivalently, $\overline{u_3^2}/u_*^2 \sim (z/L)^{2/3}$, $\overline{\theta^2}/T_*^2 \sim (z/L)^{-2/3}$. These predictions are consistent with observations (Figure 9).

Measurements also show an asymptote under the very stable conditions at $z/L \sim 1$. Its physical interpretation is that at sufficient height above the surface the rate of loss of turbulent kinetic energy to buoyancy limits the size of the largest eddies. They can no longer be as large as the distance to the surface, so z loses its significance and drops out of the governing parameter group. The scales become u_*, T_*, and L; the mean wind gradient $\partial U/\partial z$, for example, should approach u_*/L, so that $\phi_m = (kz/u_*)\partial U/\partial z \sim z/L$. This behavior is also observed [*Panofsky and Dutton*, 1984].

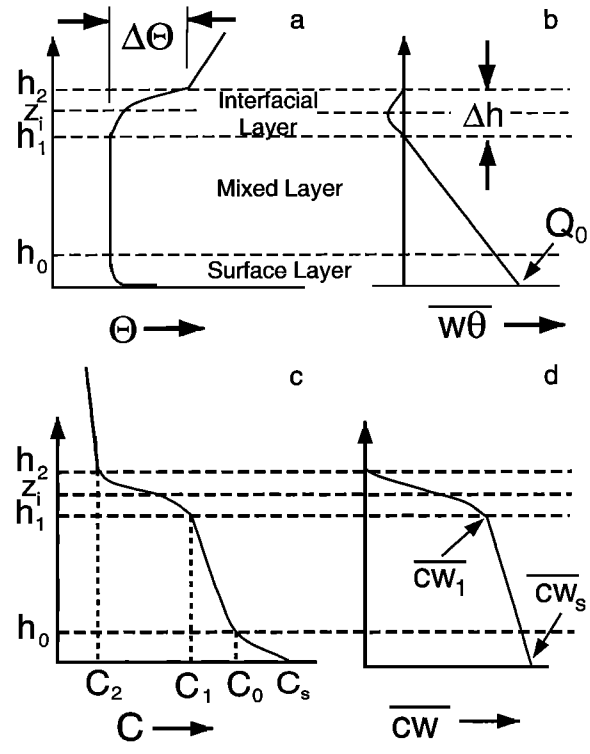

Figure 8. Mean convective boundary layer profiles of (a) potential temperature, (b) vertical temperature flux, (c) scalar mixing ratio, and (d) scalar mixing ratio flux.

The Monin-Obukhov (M-O) hypothesis has brought order to surface layer data, even at sites that are less than ideal. It does have some deficiencies; for example, it does not admit the influence of the large convective eddies. The horizontal turbulent wind field in the convective surface layer seems to scale with the convective velocity scale $w_* = (\beta Q_0 z_i)^{1/3}$ rather than u_* [*Panofsky and Dutton*, 1984]. This mechanism probably causes other deviations from M-O similarity. Another failure concerns scalar statistics. *Hill* [1989] shows that the M-O hypothesis implies that the correlation coefficient between any two conservative scalars transferred through the surface (temperature and water vapor mixing ratio, for example) is 1.0 in magnitude. Although this correlation coefficient is often observed to be large, this prediction is strictly incorrect. The M-O hypothesis neglects the surface transfer physics, which can be different for different scalars and cause some decorrelation, and also neglects other sources of scalar variance such as entrainment and horizontal inhomogeneities.

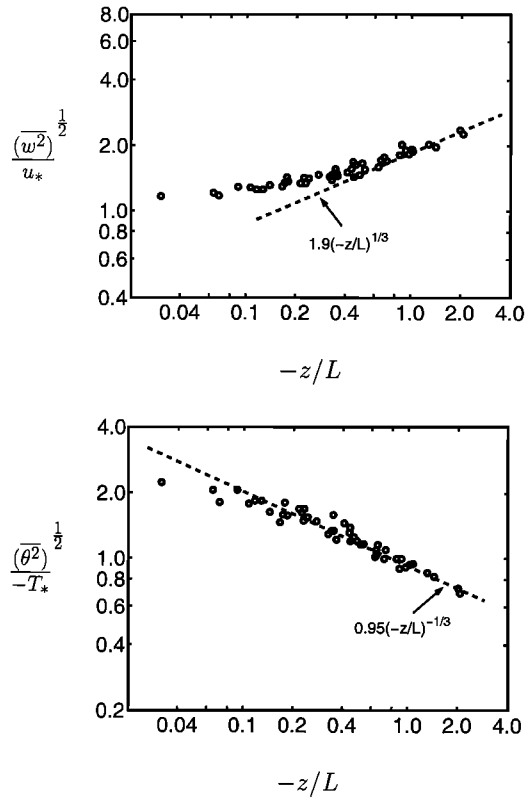

Figure 9. Kansas observations [*Wyngaard et al.*, 1971a] of the (top) rms vertical velocity and (bottom) rms temperature plotted in Monin-Obukhov coordinates.

5.3.2. Mixed layer. The midportions of the convective boundary layer are called the "mixed layer" (Figure 8) because of the strong mixing characteristics of its buoyancy-driven turbulence. (It is sometimes erroneously called the "mixing layer," a term properly reserved for the mixing region between two jets of different speed.) *Deardorff* [1970] suggested that the governing parameters for mixed-layer turbulence are β, z, z_i, Q_0, and the surface water vapor flux $\overline{wq}_s$. In this mixed-layer scaling hypothesis, statistics made dimensionless with w_*, z, a temperature scale $\theta_* = Q_0/w_*$, and a water vapor scale $q_* = \overline{wq}_s/w_*$ are universal functions of z/z_i. For example, temperature variance θ^2 is hypothesized to vary as $\theta_*^2 f(z/z_i)$, where f is a universal function. Near the bottom of the mixed layer these functions often agree with the local free convection prediction. For example, for temperature and vertical velocity variances we have $\theta^2 \sim T_f^2 \sim \theta_*^2(z/z_i)^{-2/3}$, $u_3^2 \sim u_f^2 \sim w_*^2(z/z_i)^{2/3}$, which are observed [*Panofsky and Dutton*, 1984].

As with M-O similarity, the detailed and systematic observations necessary to assess the range of validity of mixed-layer scaling do not exist. *Kustas and Brutsaert* [1987] found that over complex terrain the effects of mechanical turbulence due to the terrain could not be neglected, but others [e.g., *Huyuh et al.*, 1990] have found that over moderate terrain under sufficiently convective conditions, mixed-layer scaling did continue to hold. The entrainment at the mixed-layer top influences turbulence statistics, particularly those of scalars, well within the mixed layer [*Kaimal et al.*, 1976]. Temperature fluctuations, for example, typically follow the mixed-layer prediction only until midlayer, where they begin to increase with height because of entrainment-induced fluctuations; water vapor fluctuations, which can dominate EM refractive index fluctuations, often depart sooner. In extreme cases this can give huge scatter (Figure 10).

One way to account for entrainment effects on scalars is the top-down, bottom-up decomposition of *Moeng and Wyngaard* [1984]. A conservative scalar field c can be written as the sum of a top-down part c_t due to the entrainment flux and a bottom-up part c_b due to the surface flux. Mixed-layer scaling deals only with the latter. A simple hypothesis is that c_t scales with the flux $\overline{cw}_1$ at mixed-layer top (Figure 8), so that $c_t^2 \sim (\overline{cw}_1/w_*)_g^2(z/z_t)$. The top-down function $g(z/z_i)$ can differ from the "flip" of the bottom-up function, $f(1 - z/z_i)$. *Moeng and Wyngaard* [1984] estimated some of the top-down scaling functions through large-eddy simulation. They found that the c_t

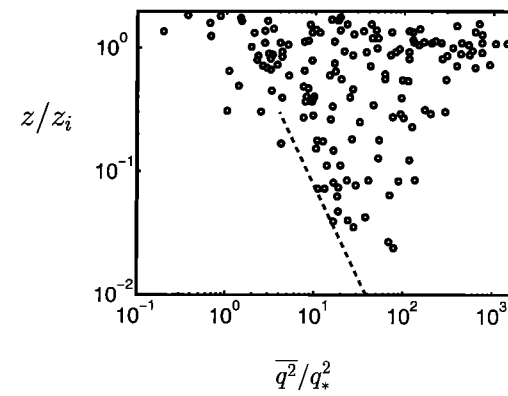

Figure 10. Mixed-layer scaling fails for water vapor mixing ratio fluctuations when their source is the entrainment process at the convective boundary layer top [*Venkatram and Wyngaard*, 1988]. Dashed line is the mixed-layer scaling found by *Kaimal et al.* [1976] for potential temperature fluctuations.

and c_b fields are correlated, so that the full variance is $\overline{c^2} = \overline{c_b^2} + 2\overline{c_b c_t} + \overline{c_t^2}$. *Fairall* [1987] used this scaling hypothesis to predict the behavior of the refractive index structure parameter in the convective boundary layer.

Observations of the truly neutral boundary layer, one with zero buoyancy flux throughout, are scarce. Rarely are adequate time and inversion-free depth available for its development to a quasi-equilibrium state. The ABL made stably stratified through a cooled surface (Figure 6) has been documented [*Caughey et al.*, 1979; *Nieuwstadt*, 1984; *Lenschow et al.*, 1988a] as has, to a lesser extent, the inversion-capped case with zero surface heat flux [*Brost et al.*, 1982; *Duynkerke and Driedonks*, 1988], which is stably stratified from above. *Nieuwstadt* [1984] has proposed a local similarity theory for the former. He suggests that the appropriate scales are based on the local kinematic shear stress and temperature flux. These define a local M-O length L_l. He hypothesizes that in analogy to M-O similarity, turbulence statistics made dimensionless with the "local" u_* and T_* are universal functions of the dimensionless height z/L_l. As a closure hypothesis, he suggests that the local turbulence Richardson number approaches a limiting constant. These notions have received support through turbulence simulation [*Mason and Derbyshire*, 1990].

5.4. Structure Function Parameters

A structure function is a two-point difference variance. For point separations $r = |r_i|$ in the inertial range of scales, and with the assumption of local isotropy, the structure function for a scalar such as refractive index n is

$$\overline{[n(x_i, t) - n(x_i + r_i, t)]^2} = C_{N^2} r^{2/3} \qquad \eta \ll r \ll \ell, \quad (25)$$

with C_{N^2} called the "structure function parameter."

Since from (8) the fluctuating refractive index n depends linearly on fluctuations of temperature and water vapor mixing ratio, it follows that [*Wyngaard et al.*, 1978]

$$C_{N^2} = a^2 C_{T^2} + 2abC_{TQ} + b^2 C_{Q^2}. \quad (26)$$

C_{T^2}, C_{Q^2}, and C_{TQ} are the temperature, water vapor, and joint structure function parameters, respectively.

Structure function parameters are ensemble-mean properties, and so vary smoothly in time and space [*Tennekes and Lumley*, 1972]. In a stationary flow they do not vary in time, and in a homogeneous flow they do not vary in homogeneous directions. In practice, however, they are invariably estimated through temporal or spatial averages, which as discussed in section 4.2 converge to the ensemble average under the proper conditions. These conditions are seldom met in atmospheric observations, and as a result, observed values of C_{N^2} often have statistical scatter that is interpreted as temporal and spatial variability. When C_{N^2} is estimated through radar returns from scattering volumes [*Gossard and Strauch*, 1983], for example, or through two-point difference variances [*Lawrence et al.*, 1970], it can appear to be a random variable.

Structure function parameters are proportional to the inertial subrange spectral level of the quantity. For temperature, for example, we can write the "experimentalist's" one-dimensional spectrum Φ^e (the one that integrates over the half line to the variance) in the inertial range as [*Wyngaard et al.* 1971b]

$$\Phi^e(\kappa_1) = 0.25 C_{T^2} \kappa_1^{-5/3}. \quad (27)$$

The solution of many propagation problems can be written as a weighted integral of the refractive index spectrum, the weighting function often being such that the inertial range of the spectrum, and therefore the refractive index structure function parameter, is dominant [*Lawrence and Strohbehn*, 1970].

In the surface layer, C_{T^2} is represented well by M-O similarity:

$$\frac{C_{T^2} z^{2/3}}{T_*^2} = f(z/L), \quad (28)$$

where f is a universal function of z/L. The value of f has been measured in the surface layer over land over a fairly wide range of z/L [*Wyngaard et al.*, 1971b]; it fits data over the ocean as well [*Davidson et al.*, 1978]. C_{Q^2} is much more difficult to measure, and data on it are relatively rare, but the observations of *Fairall et al.* [1980] indicate that it behaves much like C_{T^2}. The joint parameter C_{TQ} is nonzero only if the surface fluxes of temperature and water vapor are nonzero; its sign is the opposite of the sign of the product of these fluxes [*Wyngaard et al.*, 1978]. *Koshiek* [1982] reports measurements of all three structure function parameters in the surface layer.

Within the midportions of the convective boundary layer the structure function parameters are observed to follow mixed-layer scaling:

$$\frac{C_{T^2} z^{2/3}}{\theta_*^2} = f_1(z/z_i), \qquad \frac{C_{Q^2} z^{2/3}}{q_*^2} = f_2(z/z_i),$$

$$\frac{C_{TQ} z^{2/3}}{\theta_* q_*} = f_3(z/z_i). \tag{29}$$

The data suggest that the similarity functions are a constant multiplied by $(z/z_i)^{-4/3}$, where the constant is 2.7, 1.5, and 2.0 for f_1, f_2, and f_3, respectively [*Wyngaard and LeMone*, 1980]. Figure 11 shows observations of C_{T^2} in the convective boundary layer.

Near the top of the convective boundary layer the values of the structure function parameters typically depart from these mixed-layer forms in (29) and increase sharply to peak values before decreasing again at greater heights (Figure 11). These peaks are induced by the entrainment process and seem to be well accounted for by a simple theory [*Wyngaard and LeMone*, 1980; *Fairall*, 1987].

The behavior of the structure function parameters within the stably stratified boundary layer has been studied by *Wyngaard and Kosovic* [1994]. Using a combination of observations and large-eddy simulation, they showed evidence for a smooth transition from M-O similarity in the surface layer to the "local scaling" hypothesized by *Nieuwstadt* [1984]. They found, however, that the sensitivity of stable boundary layer structure to unsteadiness, baroclinity, terrain slope, and breaking gravity waves precludes the universality of the vertical profiles of these structure function parameters. The C_{T^2} profile is particularly sensitive.

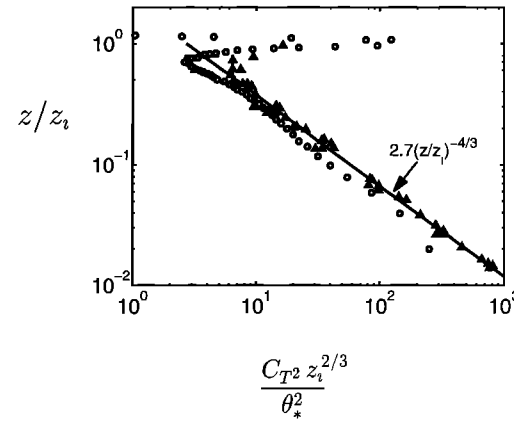

Figure 11. Vertical profiles of the temperature structure function parameter from the *Kaimal et al.* [1976] observations (triangles) and the *Peltier and Wyngaard* [1995] LES (circles). The profiles follow similar mixed-layer scaling.

6. Instantaneous Turbulent Refractive Index Fields

In the boundary layer, the only continuously turbulent part of the atmosphere, the refractive index fluctuates chaotically in time and in all three spatial directions. In EM propagation through turbulence, as in other problems impacted by turbulence, it has traditionally been felt that this complicating chaotic detail is unnecessary. For that reason, ensemble-average properties of the turbulent flow have usually been brought to such applications.

The advent of parabolic equation (PE) approaches to EM propagation has changed this situation, for the PE calls for instantaneous refractive index fields. How does one obtain three-dimensional turbulence fields? Measuring them is very difficult, if not impossible. An attractive alternative is numerical simulation.

Corrsin [1961] speculated on the role of "large computing machines" in turbulence research. After estimating that $\sim 10^{12}$ grid points would be required for a direct numerical calculation of turbulence fields from the basic fluid equations at adequately large Reynolds number (through what we now know as DNS) *Corrsin* [1961, p. 324] wrote, "The foregoing estimate is enough to suggest the use of analog instead of digital computation; in particular, how about an analog consisting of a tank of water?"

In the 1970s, *Willis and Deardorff* [1974] began a series of experiments with water in a laboratory convection tank 1 m on a side, using a layer of less dense fluid at typically 20 cm above the heated surface to cap the convection. The turbulence structure they reported bore a striking resemblance to that of the convective atmospheric boundary layer, despite its much lower Reynolds number (R_t was $\sim 4 \times 10^3$, 4 orders of magnitude less than in the atmosphere) and the absence of mean shear. This tank was used also to study the dispersion of turbulent plumes, both buoyant and nonbuoyant. Its results caused a major revamping of short-range dispersion modeling in the lower atmosphere [*Venkatram and Wyngaard*, 1988].

Despite *Corrsin*'s [1961] discouraging projection, since about 1970 there has been active interest in direct numerical simulation of turbulent flows. There has been at least as much interest in numerical modeling of turbulence. (Here we make a necessary, if not common, distinction between numerical simu-

lation and numerical modeling of turbulence. In "modeling" one represents turbulence through approximate equations (most often, equations for statistics) that display behavioral similarities to turbulence. In "simulation" one uses equations that are derivable from the exact set and hence remain faithful to the essential physics.)

Lumley [1983, p. 155] has described turbulence models as "calibrated surrogate(s) for turbulence." He cautioned against expecting more than that models should work satisfactorily in situations not too far removed geometrically, or in parameter values, from the benchmark situations used to calibrate them.

It now seems generally, if implicitly, agreed that turbulence models are not trustworthy predictors of turbulence structure in flows whose structure is not known. Furthermore, turbulence models usually produce ensemble-mean statistics, not instantaneous fields. At this time, numerical simulation offers the best path to calculating instantaneous turbulence fields.

As we discussed in section 4.3, the direct numerical solution (DNS) of the equations governing turbulent fluid motion is possible only at Reynolds numbers barely above that of transition to turbulence. Large-eddy simulation (LES) calculates the largest eddies in a turbulent flow from a spatially filtered version of the governing equations; those smaller than the numerical grid are treated very approximately through a "subgrid model."

Today's LES codes [*Moeng*, 1984; *Mason and Thomson*, 1987; *Schmidt and Schumann*, 1989; *Sykes and Henn*, 1989] are broadly similar to that pioneered by *Deardorff* [1972], although there are differences in the spatial discretization (some use spectral techniques in the horizontal, some use finite differences) and subgrid models. Today's larger computers easily allow 10^6 spatial grid points, making a $96 \times 96 \times 96$ grid, for example, quite feasible.

The difficulty of assembling suitable databases on atmospheric turbulence makes definitive testing of atmospheric LES results problematic. Most testing has been against ensemble-mean statistics from the atmosphere and from laboratory models of the atmosphere. Broadly speaking, this testing supports the fidelity of LES.

The limitations of LES include the poor performance of its subgrid model and its restriction (by computer hardware) to limited domain size. Within the boundary layer (but not too close to the capping inversion) the energy-containing range of eddies is typically well resolved by LES, so that a negligible portion of the turbulent fluxes is carried by the subgrid-scale eddies. Near the lower surface, however, this is not the case, and as a result, LES performance in the first few tens of meters can be poor.

Peltier and Wyngaard [1995] demonstrated that LES can calculate reliably the refractive index statistics in the ABL. Their profiles of structure function parameters from LES agreed well with observations in the lower portions and midportions of the convective boundary layer and in the interfacial layer (Figure 11).

7. EM Propagation: Combining Meteorology and Refractivity

7.1. Background

The traditional treatment of EM wave propagation through turbulence has two main elements: the statistical representation of refractive index turbulence and the determination of the statistical effects of this turbulence on propagating EM waves. There exists excellent documentation of the statistical structure of refractive index turbulence in the atmospheric boundary layer [*Andreas*, 1990] and the impact of meteorology on this turbulence, particularly for the inertial and dissipative spectral ranges. Since the energy-containing range of turbulence is directly impacted by buoyancy and vertical inhomogeneity, its statistical structure is more complicated and less well documented.

Parabolic equation (PE) codes for calculating EM propagation need instantaneous realizations of turbulent refractive index fields. Unfortunately, we know far more about their statistics. The Kolmogorov spectrum, the structure function parameter, local isotropy, and Monin-Obukhov and other similarity relations refer to the statistical properties of a large collection of realizations, not to properties of an actual, realizable atmospheric boundary layer. How can one use the hard-earned statistical results of micrometeorologists to generate optimally realistic turbulent refractive index fields for calculating EM propagation?

7.2. Generating Refractivity Fields From LES

The LES requirement that the energy-containing range of spatial scales be resolved, plus the current computational limit of 100–200 grid points per spatial coordinate direction, limits ABL domains to ~10 km

in the horizontal. In many propagation applications one needs domains perhaps an order of magnitude larger. That can be accomplished by coupling LES with mesoscale modeling.

One key to such coupling is that EM refractive index, being determined essentially by temperature and water vapor, is governed by linear differential equations whose solutions are superposable. Thus we write the turbulent water vapor mixing ratio field q, for example, in the ABL as

$$q(x_i, t) = q^t(x_i, t) + q^b(x_i, t) + q^{lc}(x_i, t). \quad (30)$$

Here q^t and q^b are the top-down and bottom-up turbulent fields, respectively [*Moeng and Wyngaard*, 1984]; q^t is the turbulent field generated by the entrainment process at the boundary layer top. The air above the boundary layer is usually drier than the air within the boundary layer, and entrainment in the presence of a q change across the top generates q turbulence below. The turbulent field q^b is generated by a surface flux, either from the surface to the air or vice versa; either changes the q field above. The q^{lc} (lc for "log chipper") is the turbulent q field induced by the horizontal advection of very large scale (relative to z_i) horizontal q gradients, which are "chewed up" by the turbulent velocity field and can contribute significantly to the turbulent q field in the boundary layer. We have studied q^{lc} through large-eddy simulation [*Kimmel and Wyngaard*, 2001].

Each of the q^t, q^b, and q^{lc} fields can be written as the sum of a mean part and a fluctuating part. The mean is traditionally the ensemble mean, not a spatial mean or a time mean. It can be approximated by the mesoscale resolvable-scale field, the low-pass spatially filtered field with cutoff in the mesoscale, at a scale of a few kilometers to a few tens of kilometers, say. The fluctuating (turbulent) part is the deviation from the mean. By definition it is three-dimensionally irregular, time dependent, and random.

The mean part of q is important for ducted propagation. In principle it can be calculated adequately with a mesoscale model, although the model may have to be redesigned for this purpose [*Otte et al.*, 1996]. For nonducted propagation, where EM troposcatter can be important, the critical part is the fluctuating refractive index field not resolved by the mesoscale model.

In order to provide the refractive index input for a PE solver, the mesoscale model, having horizontal grid scale Δ_h and vertical scale Δ_v, needs a subgrid-scale refractive index field within the ABL. LES of the boundary layer on a horizontal domain of length Δ_h provides the refractive index field on horizontal scales from Δ_h down to the LES resolution δ, which is typically a few tens of meters. If the LES refractive index fields are calculated for the conditions in the mesoscale grid element $\Delta_h \times \Delta_h \times \Delta_v$, then the linearity of the refractive index conservation equation allows us to add the LES and mesoscale refractive index fields.

Running LES on demand in this way is wildly impractical, so such "brute force" superposition is out of the question. The simple similarity expressions of *Moeng and Wyngaard* [1984] suggest an alternative. They wrote, for the convective boundary layer,

$$q^t = \frac{\overline{wq}_1}{w_*} f^t, \qquad q^b = \frac{\overline{wq}_s}{w_*} f^b, \quad (31)$$

where $\overline{wq}_1$ and $\overline{wq}_s$ are the q fluxes at the ABL top and bottom, respectively (Figure 8), w_* is the turbulent velocity scale for the boundary layer, and the f are dimensionless random functions. There is some interesting physics in the f; for example, f^t and f^b are strongly correlated [*Moeng and Wyngaard*, 1984]. *Kimmel and Wyngaard* [2001] propose an analogous expression for the log chipper component.

Because of the sensitive dependence of turbulence on initial conditions the f functions in a given realization of the ABL are unpredictable in detail. A statistically representative f for a given type of ABL can be chosen from a small set (10, say) that has been precalculated through LES and archived. In this way the q fields in a realization of a given type of ABL can be generated by appropriately scaling the archived f for that type of ABL. A small set of f makes it possible to generate several realizations.

To pursue this approach, one needs to know the minimum set of representative boundary layer states (e.g., very convective, weakly convective, inversion-capped neutral, slightly stable, very stable). For each state one needs a small set of f fields generated through LES and a similarity formulation for the refractive index components (e.g., (31) for the convective state) in order to scale these f functions for applications.

A question naturally arises: Is this range-dependent detail needed in order to calculate troposcatter reliably? Could the fine structure instead be added through fine-vertical-resolution radiosonde profiles that do not include fine structure in range?

In simulating EM propagation in the variation of coastal atmospheric refractivity (VOCAR) experiment [*Paulus*, 1994], *Gilbert et al.* [1999] compared results for this plywood approximation (refractive index that varies in the vertical but not in range) and for refractivity with three-dimensional variations calculated through LES. With the plywood approximation, signal levels were typically 15–20 dB higher, and the horizontal and vertical coherences of the EM field were much greater than one would expect in a turbulent atmosphere.

Curiously, however, *Gilbert et al.* [1999] found that despite its unphysicality the plywood approximation gave signal levels that fit those observed in VOCAR. They inferred that a neglected physical mechanism was responsible for the observed VOCAR levels. Their hypothesized mechanism was the sharp change in the water vapor mixing ratio across the local, instantaneous, horizontally varying top of the ABL. It appears that LES cannot easily resolve this top to the detail necessary for PE calculations of forward scatter of EM waves. *Gilbert et al.* [1999] instead modeled the instantaneous, local ABL top by assuming that the observed change in refractive index at the top occurred over a depth of a few meters and that the top height varied randomly with range with an integral scale of the order of the ABL depth. With this model their PE calculations fit the VOCAR data.

Plate 1 illustrates the effect of the ABL top on propagation at 0.263 GHz calculated through a PE model [*Gilbert and Di*, 1993; *Gilbert et al.*, 1999]. In Plate 1a the refractivity and trapping-layer height fields for the PE model were obtained directly from a mesoscale model having 12 km horizontal resolution and 40 m vertical resolution. The trapping-layer thickness indicated by the mesoscale model's predicted moisture and temperature fields varied between ~40 m and 120 m along the propagation path. Plate 1a indicates fairly strong signal strength along the surface for most of the range.

Plate 1b presents the propagation factor for the mesoscale fields used in Plate 1a but augmented with stochastic, range-dependent fluctuations in trapping-layer height. The horizontal correlation length of these fluctuations was taken as z_i, and the rms amplitude was $0.033\ z_i$. As Plate 1b shows, this significantly lowered the near-surface signal strength in the middle of the range, between 40 and 100 km.

Plate 1c shows the propagation factor when the trapping-layer thickness from the mesoscale model is stochastically compressed to give a better representation of the sharp, random top characteristic of the convective boundary layer. The mean trapping-layer thickness was 3 m, and its rms fluctuation was 1 m. The trapping-layer height retained the range-dependent fluctuations used in Plate 1b. This dramatically raised the near-surface propagation factor at all ranges beyond 40 km. These examples indicate that even when realistic spatial variability is added to the trapping-layer height, the sharpness of the layer (i.e., its reduced thickness) caused by convective turbulence can greatly enhance received signal strength.

7.3. Local, Instantaneous Top of the ABL

Corrsin and Kistler [1954] argued that the free-stream boundaries of turbulent flows are made quite sharp by the stretching of vorticity on the turbulent side of the boundary. They estimated the thickness of the laminar superlayer at a free-stream boundary as on the order of the Kolmogorov microscale η. *LaRue and Libby* [1976, 1981] used fine-wire probes to measure the thickness of instantaneous boundaries of laboratory turbulent airflows. In the wake of a heated cylinder the mean thickness was $8\ \eta_\theta$; in the thermal mixing layer downstream of a half-heated turbulence grid it was $12\ \eta_\theta$. Here $\eta_\theta = (\gamma/\nu)^{1/2}\ \eta$ is the Kolmogorov microscale for temperature; in air, $\eta_\theta \simeq 1.2\ \eta$. Thus the LaRue and Libby data indicate a mean local interface thickness in air in the range $10–15\ \eta$.

The ABL top is a free-stream boundary between the turbulent ABL air and the nonturbulent air above. If we do not normally think of the ABL top as being sharp, it is no doubt in part because we tend to think of average properties of turbulent flows, not instantaneous ones. The Gaussian plume is a familiar model for the mean concentration distribution downwind of a point source, but it is a poor model of the instantaneous concentration profile.

Remote sensors such as the acoustic sounder [*Neff and Coulter*, 1986] and lidar [*Schwiesow*, 1986] can reveal the sharp demarcation between the turbulent ABL and the nonturbulent flow above, but there has been surprisingly little quantitative documentation of the structure of this instantaneous ABL top. Radiosonde signals, even from sensors with sufficient frequency response, are not usually processed with enough temporal resolution to reveal its full sharpness.

One exception has been the long series of helicop-

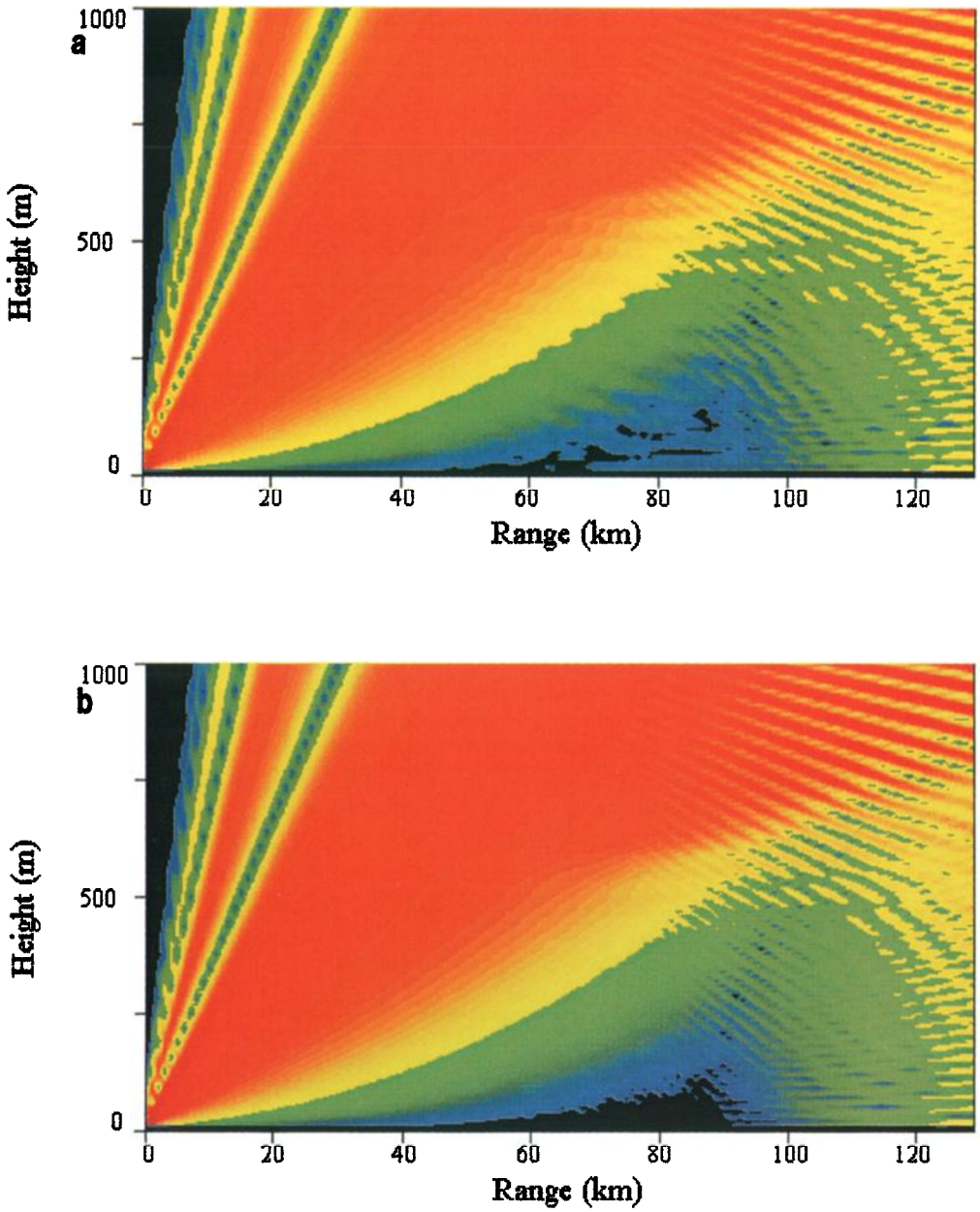

Plate 1. Color plots of the propagation factor versus range and height (0.263 GHz) for a range interval of 0–130 km. The source height is 18.4 m, and there is an elevated trapping layer at 540 m. (a) Calculations using the mean refractivity field from a mesoscale model solution. (b) Calculations using the mean refractivity field from a mesoscale model solution plus random, range-dependent fluctuations in the trapping-layer height. (c) As in Plate 1b, but the interfacial layer depth was compressed to a mean of 3 m with a random, range-dependent rms fluctuation of 1 m.

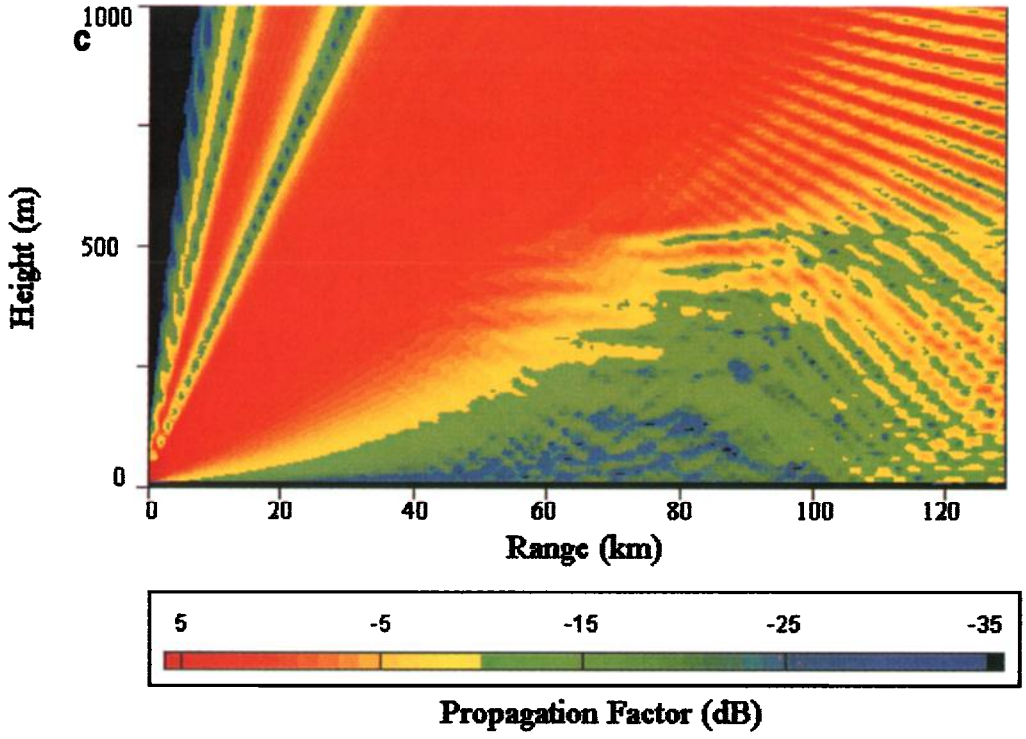

Plate 1. (continued)

ter flights carried out by the Johns Hopkins University Applied Physics Laboratory in the marine boundary layer [*Babin and Rowland*, 1992]. The sensors included specially prepared VIZ Premium carbon film humidity elements with a response time of 0.5 s at 25°C and a thermistor with a 0.5 s response time. Altitude was measured with a dual-beam radar altimeter with a resolution of 0.3 m. The sampling rate, forward airspeed, and descent rate were such that rotor downwash was well behind the sensors and the vertical resolution of the temperature and moisture profiles was between 0.75 m and 1.5 m.

Figure 12 shows an instantaneous, unaveraged profile of virtual potential temperature measured in this program. This sounding was made off the California coast, ~20 km northwest of San Nicolas Island and ~102 km southwest of Point Mugu. The wind was out of the northeast, the skies were partly cloudy, and the seas were calm. There was a high over the California desert with Santa Ana conditions. The virtual potential temperature profile of Figure 12 indicates that the boundary layer was stably stratified. Stable stratification strongly affects the structure of a turbulent boundary layer, eliminating the largest eddies and gradually attenuating the turbulence intensity with height until it is extinguished. As a result the instantaneous top of a stably stratified ABL is rather diffuse: not as sharp, we believe, as that of a typical convective ABL.

Available data on the structure function parameters of temperature and humidity indirectly support the notion of a sharp local top of the convective ABL. Figure 13, top panel, shows the pronounced peak in the vertical profile of C_{Q^2} near z_i as reported by *Wyngaard and LeMone* [1980]. Their prediction of the interfacial-layer-averaged value of this peak in C_{Q^2} seems successful (lower panel). This is referred to as the entrainment-induced peak, but it receives contributions also from the random vertical motion of a sharp top having a significant change in humidity across it.

Lenschow et al. [1988b] measured temperature and ozone mixing ratio at the local top of a stratocumulus-topped convective ABL. Their data were obtained on horizontal flight paths and analyzed through a compositing technique. They presented the ensemble-average profiles of temperature and ozone mixing

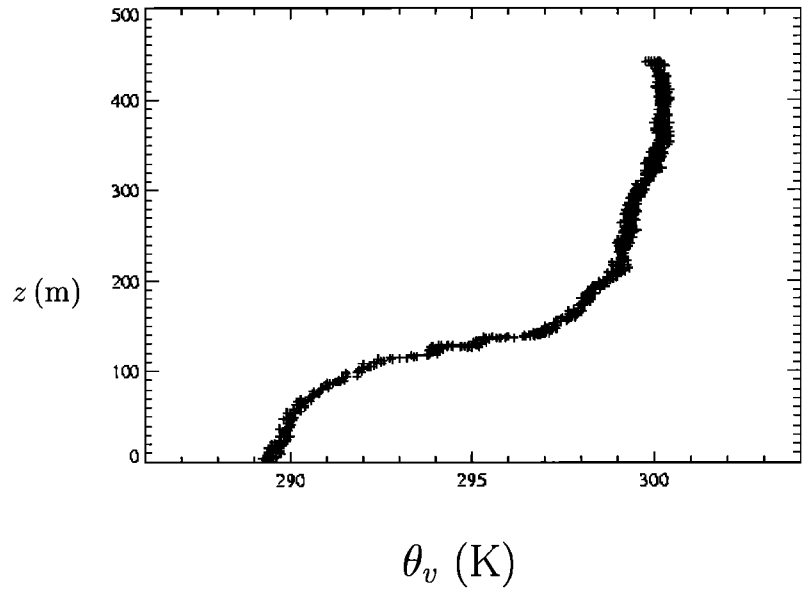

Figure 12. An instantaneous, unaveraged profile of virtual potential temperature in a stably stratified boundary layer off the California coast [*Babin and Rowland*, 1992]. We attribute the relatively diffuse nature of the instantaneous top to the stable stratification of the boundary layer.

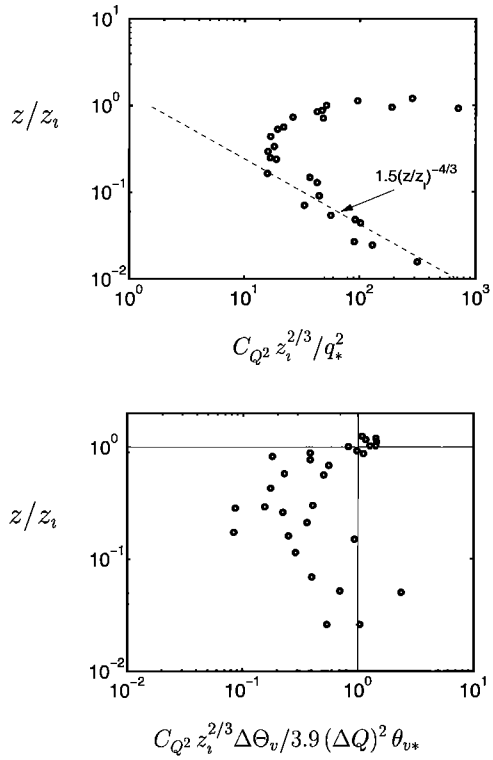

Figure 13. Mixed-layer scaling describes the data within the lower part of the mixed layer (top plot), but different scaling is required to collapse the data in the interfacial layer (bottom plot) [*Wyngaard and LeMone*, 1980].

ratio in the immediate vicinity of the local top. Their sensors and sampling rates gave a vertical resolution of 0.3 m in these profiles. Their results, Figure 13, suggest an instantaneous top thickness of perhaps 3 m. The changes in temperature and ozone mixing ratio across this top were each ~1/6 of the full difference (the difference between the mean mixed-layer value and the value in the overlying free atmosphere), which is not evident in Figure 14.

Laboratory flows typically have R_t (turbulence Reynolds number) values in the range 10^3–10^4, while the convective ABL typically has $R_t \sim 10^8$ (section 4). The details of scalar turbulence at 1–100 m scales, say, in the ABL are strongly influenced by the turbulent velocity field at these scales. In the midportions and upper portions of the ABL these scales lie in the inertial range, where statistics differ greatly in the *Kolmogorov* [1941] hypothesis and the revised version [*Kolmogorov*, 1962].

We can illustrate this difference in statistics with a squared two-point velocity difference $[u(\mathbf{x}, t) - u(\mathbf{x} + r, t)]^2$ averaged over a volume of the order of r^3, where $r \gg \eta$. By the *Kolmogorov* [1941] hypothesis, ensemble statistics of this volume-averaged quantity depend only on ε and r; the ensemble mean goes as $\varepsilon^{2/3} r^{2/3}$, and the variance goes as $\varepsilon^{4/3} r^{4/3}$. Thus the ratio of the variance and the square of the ensemble

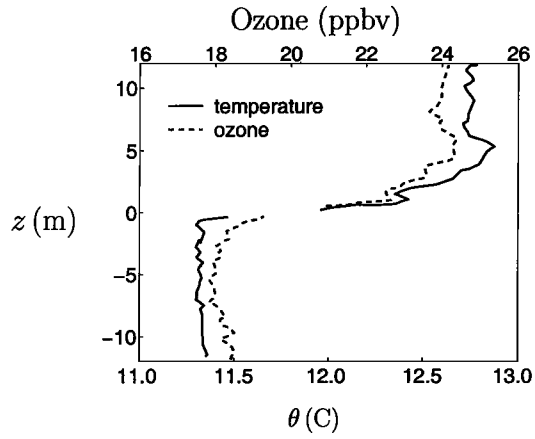

Figure 14. Aircraft measurements [*Lenschow et al.*, 1988b] illustrating the sharpness of the local, instantaneous top of a cloud-topped convective boundary layer. Here z is measured from the mean top.

mean is predicted to be a constant. By the *Kolmogorov* [1962] hypothesis the ensemble mean goes as $\overline{\tilde{\varepsilon}^{2/3}} r^{2/3}$, where $\tilde{\varepsilon}$ is the instantaneous, local dissipation rate averaged over the volume r^3; the variance goes as $\overline{\tilde{\varepsilon}^{4/3}} r^{4/3}$. As a result the ratio of the variance and the square of the ensemble mean goes as $\overline{\tilde{\varepsilon}^{4/3}}/(\overline{\tilde{\varepsilon}^{2/3}})^2$. In the 1962 hypothesis this increases with l/r, indicating increasing intermittency of a locally averaged quantity with increasing l/r. This has been borne out by observations [*Antonia et al.*, 1984].

The ratio of the scale l of the large, flow-spanning, ABL-top-distorting eddies and the scale η of the dissipative eddies and of the *Corrsin and Kistler* [1954] laminar superlayer goes as $R_t^{3/4}$ (section 4.3). The eddies at the smaller-scale end of this range are much more intermittent in the high-R_t ABL than in much lower R_t laboratory flows. It is reasonable to expect this higher intermittency to lead to a structurally more complicated free-stream boundary of a turbulent flow as R_t increases. Perhaps at very large R_t the local ABL top, the local boundary between turbulent and nonturbulent flow, disintegrates into a local field of boundaries, a "lacy" boundary. This is consistent with the *Lenschow et al.* [1988b] finding that the difference in scalar across the local top of a convective ABL was a small fraction of the overall difference.

Kiemle et al. [1998] have presented airborne lidar backscatter measurements made near the top of a convective ABL that has substantial mean wind shear. The backscatter is from aerosols, whose concentration tends to be larger in the ABL than in the nonturbulent air above. The average thickness of the local layer across which the full difference occurs, which they label the "entrainment zone," is 100–150 m. This is consistent with the high-resolution plot of aerosol concentration in a vertical plane shown in Figure 15. While the instantaneous ABL top appears sharp, it appears that only a portion of the overall concentration difference occurs across it. Perhaps this

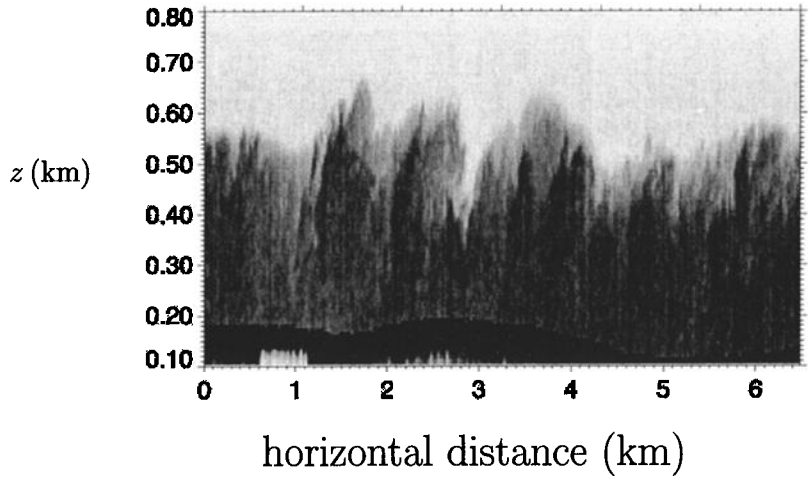

Figure 15. Airborne lidar measurements of aerosol concentration in a vertical plane of a convective boundary layer with substantial mean wind shear [*Kiemle et al.*, 1998]. The instantaneous top is quite irregular, and it appears that only a portion of the overall jump in aerosol concentration occurs across it.

is a property of a "lacy" instantaneous ABL top of the convective atmospheric boundary layer.

It seems clear that more research needs to be done on the nature of the local, instantaneous top of the convective ABL, its dependence on meteorological conditions and on the global properties of the boundary layer, and its impact on forward scattering of EM waves.

Acknowledgments. This work was supported in part by the U.S. Navy under contract N00039-92-C-0100 and under SPAWAR research contract N00039-97-D-0042 and by the Army Research Office through grant DAAG55-97-1-0296 P00001. We are grateful to Steve Fast, Ted Rogers, and Walter A. Bach for this support and for their encouragement. We are also grateful to Steve Babin of the Johns Hopkins University Applied Physics Laboratory, Don Lenschow of NCAR, and Ken Davis of Penn State for helpful discussions and for granting us the use of Figures 12, 14, and 15, respectively.

References

Andreas, E. L., Ed., *Turbulence in a Refractive Medium*, *SPIE Milestone Ser., MS 25*, 693 pp., 1990.

Antonia, R. A., E. J. Hopfinger, Y. Gagne, and F. Anselmet, Temperature structure functions in turbulent shear flows, *Phys. Rev. A, 30*, 2704–2707, 1984.

Babin, S. M., and J. R. Rowland, Observation of a strong surface radar duct using helicopter acquired fine-scale radio refractivity measurements, *Geophys. Res. Lett., 19*, 917–920, 1992.

Batchelor, G. K., *The Theory of Homogeneous Turbulence*, 197 pp., Cambridge Univ. Press, New York, 1960.

Black, T. L., NMC notes: The new NMC Mesoscale Eta Model: Description and forecast experiments, *Weather Forecasting, 2*, 266–278, 1994.

Brost, R. A., J. C. Wyngaard, and D. H. Lenschow, Marine stratocumulus layers, part II, Turbulence budgets, *J. Atmos. Sci., 38*, 818–836, 1982.

Burk, S. D., and W. T. Thompson, Mesoscale modeling of summertime refractive conditions in the Southern California Bight, *J. Appl. Meteorol., 36*, 22–31, 1997.

Caughey, S. J., J. C. Wyngaard, and J. C. Kaimal, Turbulence in the evolving stable boundary layer, *J. Atmos. Sci., 36*, 1041–1052, 1979.

Champagne, F. H., C. A. Friehe, J. C. LaRue, and J. C. Wyngaard, Flux measurements, flux-estimation techniques, and fine-scale turbulence measurements in the unstable surface layer over land, *J. Atmos. Sci., 34*, 515–530, 1977. (Reproduced in *Turbulence in a Refractive Medium*, edited by E. L. Andreas, *SPIE Milestone Ser., MS 25*, 148–163, 1990.)

Corrsin, S., On the spectrum of isotropic temperature fluctuations in isotropic turbulence, *J. Appl. Phys., 22*, 469–473, 1951. (Reproduced in *Turbulence in a Refractive Medium*, edited by E. L. Andreas, *SPIE Milestone Ser., MS 25*, 75–79, 1990.)

Corrsin, S., Turbulent flow, *Am. Sci., 49*, 300–325, 1961.

Corrsin, S., and A. Kistler, Free-stream boundaries of turbulent flows, *NACA Rep. 1244*, NASA Cent. for Aerosp. Inf., Hanover, Md., 1954.

Davidson, K. L., T. M. Houlihan, C. W. Fairall, and G. E. Schacher, Observation of the temperature structure-function parameter, C_T^2, over the ocean, *Boundary Layer Meteorol., 15*, 507–523, 1978. (Reproduced in *Turbulence in a Refractive Medium*, edited by E. L. Andreas, *SPIE Milestone Ser., MS 25*, 422–438, 1990.)

Deardorff, J. W., Convective velocity and temperature scales for the unstable planetary boundary layer and for Rayleigh convection, *J. Atmos. Sci., 27*, 1211–1213, 1970.

Deardorff, J. W., Numerical investigation of neutral and unstable planetary boundary layers, *J. Atmos. Sci., 29*, 91–115, 1972.

Dockery, G. D., Modeling electromagnetic wave propagation in the troposphere using the parabolic equation, *IEEE Trans. Antennas Propag., 36*(10), 1464–1470, 1988.

Dockery, G. D., Development and use of electromagnetic parabolic equation propagation models for U.S. Navy applications, *Johns Hopkins APL Tech. Dig., 19*, 283–292, 1998.

Dudhia, J., A nonhydrostatic version of the Penn State/NCAR mesoscale model: Validation tests and simulations of an Atlantic cyclone and cold front, *Mon. Weather Rev., 121*, 1493–1513, 1993.

Durran, D. R., *Numerical Methods for Wave Equations in Geophysical Fluid Dynamics*, 465 pp., Springer-Verlag, New York, 1998.

Duynkerke, P. G., and A. G. M. Driedonks, Turbulent structure of a shear-driven stratus-topped atmospheric boundary layer: A comparison of model results with observations, *J. Atmos. Sci., 45*, 2343–2351, 1988.

Fairall, C. W., A top-down and bottom-up diffusion model of C_T^2 and C_Q^2 in the entraining convective boundary layer, *J. Atmos. Sci., 44*, 1009–1017, 1987. (Reproduced in *Turbulence in a Refractive Medium*, edited by E. L. Andreas, *SPIE Milestone Ser., MS 25*, 464–472, 1990.)

Fairall, C. W., G. E. Schacher, and K. L. Davidson, Measurements of the humidity structure-function parameters, C_q^2 and C_{Tq}, over the ocean, *Boundary Layer Meteorol., 19*, 81–92, 1980. (Reproduced in *Turbulence in a Refractive Medium*, edited by E. L. Andreas, *SPIE Milestone Ser., MS 25*, 439–444, 1990.)

Fox, D. G., and D. K. Lilly, Numerical simulation of turbulent flows, *Rev. Geophys., 10*, 51–72, 1972.

Galperin, B., and S. A. Orszag, Eds., *Large Eddy Simulation of Complex Engineering and Geophysical Flows*, 600 pp., Cambridge, Univ. Press, New York, 1993.

Gilbert, K. E., and X. Di, A fast Green's function method

for one-way sound propagation in the atmosphere, *J. Acoust. Soc. Am.*, *94*, 2343–2352, 1993.

Gilbert, K. E., X. Di, S. Khanna, M. Otte, and J. C. Wyngaard, Electromagnetic wave propagation through simulated atmospheric refractivity fields, *Radio Sci.*, *34*, 1413–1435, 1999.

Gossard, E. E., and R. G. Strauch, *Radar Observation of Clear Air and Clouds*, 280 pp., Elsevier Sci., New York, 1983.

Haugen, D. A., J. C. Kaimal, and E. F. Bradley, An experimental study of Reynolds stress and heat flux in the atmospheric surface layer, *Q. J. R. Meteorol. Soc.*, *97*, 168–180, 1971.

Hill, R. J., Models of the scalar spectrum for turbulent advection, *J. Fluid Mech.*, *88*, 541–562, 1978a. (Reproduced in *Turbulence in a Refractive Medium*, edited by E. L. Andreas, *SPIE Milestone Ser.*, *MS 25*, 80–101, 1990.)

Hill, R. J., Spectra of fluctuations in refractivity, temperature, humidity, and the temperature-humidity cospectrum in the inertial and dissipation ranges, *Radio Sci.*, *13*, 953–961, 1978b. (Reproduced in *Turbulence in a Refractive Medium*, edited by E. L. Andreas, *SPIE Milestone Ser.*, *MS 25*, 102–110, 1990.)

Hill, R. J., Implications of Monin-Obukhov similarity theory for scalar quantities, *J. Atmos. Sci.*, *46*, 2236–2244, 1989.

Hitney, H. V., A practical troposcatter model using the parabolic equation, *IEEE Trans. Antennas Propag.*, *41*, 905–909, 1993.

Hodur, R. M., The Naval Research Laboratory's Coupled Ocean/Atmosphere Mesoscale Prediction System (COAMPS), *Mon. Weather Rev.*, *125*, 1414–1430, 1987.

Hunt, J. C. R., Some connections between fluid mechanics and the solving of industrial and environmental fluid-flow problems, *J. Fluid Mech.*, *106*, 103–130, 1981.

Huyuh, B. P., C. E. Coulman, and T. R. Turner, Some turbulence characteristics of convectively mixed layers over rugged and homogeneous terrain, *Boundary Layer Meteorol.*, *51*, 229–254, 1990.

Kaimal, J. C., and J. Finnigan, *Atmospheric Boundary Layer Flows*, 304 pp., Oxford, Univ. Press, New York, 1994.

Kaimal, J. C., J. C. Wyngaard, D. A. Haugen, O. R. Coté, Y. Izumi, S. J. Caughey, and C. J. Readings, Turbulence structure in the convective boundary layer, *J. Atmos. Sci.*, *33*, 2152–2169, 1976. (Reproduced in *Turbulence in a Refractive Medium*, edited by E. L. Andreas, *SPIE Milestone Ser.*, *MS 25*, 353–370, 1990.)

Kiemle, C., G. Ehter, and K. Davis, Airborne lidar studies of the entrainment zone, in *Proceedings of the 19th International Laser-Radar Conference, July, 1998, Annapolis, Maryland*, edited by U. N. Singh, S. Ismail, and G. K. Schwemmer, *NASA Conf. Publ., NASA/CP-1998-207671/PT1*, 395–398, 1998.

Kimmel, S., and J. C. Wyngaard, "Log-chipper" turbulence in the convective boundary layer, *J. Atmos. Sci.*, in press, 2001.

Kolmogorov, A. N., The local structure of turbulence in incompressible viscous fluid for very large Reynolds numbers, *C. R. Hebd. Seances Acad. Sci.*, *30*, 301–305, 1941.

Kolmogorov, A. N., A refinement of previous hypotheses concerning the local structure of turbulence in a viscous incompressible fluid at high Reynolds number, *J. Fluid Mech.*, *13*, 82–85, 1962.

Koshiek, W., Measuring C_T^2, C_Q^2 and C_{TQ} in the unstable surface layer, and relations to the vertical fluxes of heat and moisture, *Boundary Layer Meteorol.*, *24*, 89–107, 1982. (Reproduced in *Turbulence in a Refractive Medium*, edited by E. L. Andreas, *SPIE Milestone Ser.*, *MS 25*, 445–463, 1990.)

Kustas, W. P., and W. Brutsaert, Budgets of water vapor in the unstable boundary layer over rugged terrain, *J. Clim. Appl. Meteorol.*, *26*, 607–620, 1987.

Kuttler, J. R., and G. D. Dockery, Theoretical description of the PE/Fourier splitstep method of representing electromagnetic propagation in the troposphere, *Radio Sci.*, *26*, 381–303, 1991.

LaRue, J. C., and P. A. Libby, Statistical properties of the interface in the turbulent wake of a heated cylinder, *Phys. Fluids*, *19*, 1864–1875, 1976.

LaRue, J. C., and P. A. Libby, Thermal mixing layer downstream of a half-heated turbulence grid, *Phys. Fluids*, *24*, 597–603, 1981.

Lawrence, R. S., and J. W. Strohbehn, A survey of clear-air propagation effects relevant to optical communications, *Proc. IEEE*, *58*, 1523–1545, 1970. (Reproduced in *Turbulence in a Refractive Medium*, edited by E. L. Andreas, *SPIE Milestone Ser.*, *MS 25*, 22–44, 1990.)

Lawrence, R. S., G. R. Ochs, and S. F. Clifford, Measurements of atmospheric turbulence relevant to optical propagation, *J. Opt. Soc. Am.*, *60*, 826–830, 1970. (Reproduced in *Turbulence in a Refractive Medium*, edited by E. L. Andreas, *SPIE Milestone Ser.*, *MS 25*, 475–479, 1990.)

Lenschow, D. H., X. S. Li, C. J. Zhu, and B. B. Stankov, The stably stratified boundary layer over the Great Plains, 1, Mean and turbulence structure, *Boundary Layer Meteorol.*, *42*, 95–122, 1988a.

Lenschow, D. H., V. Patel, and A. Isbell, Measurements of fine-scale structure at the top of marine stratocumulus, paper presented at Eighth Symposium on Turbulence and Diffusion, Am. Meteorol. Soc., Boston, Mass., 1988b.

Lumley, J. L., Atmospheric modelling, *Mech. Eng. Trans.*, *ME8*, 153–159, 1983.

Lumley, J. L. and H. A. Panofsky, *The Structure of Atmospheric Turbulence*, 239 pp., Wiley-Interscience, New York, 1964.

Mason, P. J., and S. H. Derbyshire, Large-eddy simulation

of the stably stratified atmospheric boundary layer, *Boundary Layer Meteorol., 53*, 117–162, 1990.

Mason, P. J., and D. J. Thomson, Large-eddy simulation of the neutral-static-stability planetary boundary layer, *Q. J. R. Meteorol. Soc., 113*, 413–443, 1987.

McAllister, L. G., Acoustic sounding of the lower troposphere, *J. Atmos. Terr. Phys., 30*, 1439–1440, 1968.

Moeng, C.-H., A large-eddy-simulation model for the study of planetary boundary layer turbulence, *J. Atmos. Sci., 41*, 2052–2062, 1984.

Moeng, C.-H., and J. C. Wyngaard, Statistics of conservative scalars in the convective boundary layer, *J. Atmos. Sci., 41*, 3161–3169, 1984. (Reproduced in *Turbulence in a Refractive Medium*, edited by E. L. Andreas, *SPIE Milestone Ser., MS 25*, 407–415, 1990.)

Neff, W. D., and R. L. Coulter, Acoustic remote sounding, in *Probing the Atmospheric Boundary Layer*, edited by D. H. Lenschow, pp. 201–239, Am. Meteorol. Soc. Boston, Mass., 1986.

Nieuwstadt, F. T. M., The turbulent structure of the stable nocturnal boundary layer, *J. Atmos. Sci., 41*, 2202–1226, 1984.

Obukhov, A. M., Structure of the temperature field in turbulent flow, *Izv. Akad. Nauk SSSR, Ser. Geogr. Geofiz., 13*(1), 58–69, 1949. (Reproduced in *Turbulence in a Refractive Medium*, edited by E. L. Andreas, *SPIE Milestone Ser., MS 25*, 65–74, 1990.)

Otte, M., N. Seaman, D. Stauffer, and J. C. Wyngaard, A mesoscale model for EM ducting in the marine boundary layer, in *Proceedings of the 1996 Battlespace Atmospherics Conference, NRAD Tech. Doc. 2938*, 622 pp., Space and Nav. Warfare Syst. Cent., San Diego, Calif., 1996.

Panofsky, H. A., and J. A. Dutton, *Atmospheric Turbulence*, 397 pp., John Wiley, New York, 1984.

Paulus, R. A., VOCAR: An experiment in the variability of coastal atmospheric refractivity, paper presented at International Geoscience and Remote Sensing Symposium, Calif. Inst. of Technol., Pasadena, Aug. 8–12, 1994.

Peltier, L. J., and J. C. Wyngaard, Structure-function parameters in the convective boundary layer from large-eddy simulation, *J. Atmos. Sci., 52*, 3641–3660, 1995.

Pielke, R. A., et al., A comprehensive meteorological modeling system: RAMS, *Meteorol. Atmos. Phys., 49*, 69–91, 1992.

Reynolds, O., On the dynamical theory of incompressible viscous fluids and the determination of the criterion, *Philos. Trans. R. Soc. London, Ser. A, 186*, 123–164, 1895.

Rogallo, R. S., and P. Moin, Numerical simulation of turbulent flows, *Annu. Rev. Fluid Mech., 16*, 99–137, 1984.

Rogers, L. T., Demonstration of an efficient boundary layer parameterization for unbiased propagation estimation, *Radio Sci., 33*, 1599–1608, 1998.

Schmidt, H., and U. Schumann, Coherent structure of the convective boundary layer deduced from large-eddy simulation, *J. Fluid Mech., 200*, 511–562, 1989.

Schwiesow, R. L., Lidar measurement of boundary-layer variables, in *Probing the Atmospheric Boundary Layer*, edited by D. H. Lenschow, pp. 139–162, Am. Meteorol. Soc., Boston, Mass., 1986.

Scorer, R. S., Book review, *Clean Air, 10*, 148–149, 1980.

Seaman, N. L., and D. R. Stauffer, Influence of turbulence parameterization on the structure of the coastal sea breeze in the Persian Gulf, paper presented at 3rd Conference on Coastal Atmospheric and Ocean Prediction Processes, Am. Meteorol. Soc., New Orleans, La., Nov. 3–5, 1999.

Sreenivasan, K. R., Local isotropy of passive scalars in turbulent flows, *Proc. R. Soc. London, Ser. A, 434*, 165–182, 1991.

Strohbehn, J. W., Line-of-sight wave propagation through the turbulent atmosphere, *Proc. IEEE, 56*, 1301–1318, 1968. (Reproduced in *Turbulence in a Refractive Medium*, edited by E. L. Andreas, *SPIE Milestone Ser., MS 25*, 3–21, 1990.)

Stull, R., *An Introduction to Boundary Layer Meteorology*, 402 pp., Kluwer Acad., Norwell, Mass., 1988.

Sykes, R. I., and D. S. Henn, Large-eddy simulation of turbulent sheared convection, *J. Atmos. Sci., 46*, 1106–1118, 1989.

Taylor, G. I., Statistical theory of turbulence, part I, *Proc. R. Soc. London, Ser. A, 151*, 421–444, 1935a.

Taylor, G. I., Statistical theory of turbulence, part II, Measurements of correlation in the Eulerian representation of turbulent flow, *Proc. R. Soc. London, Ser. A, 151*, 445–454, 1935b.

Taylor, G. I., Statistical theory of turbulence, part III, Distribution of dissipation of energy in a pipe over its cross-section, *Proc. R. Soc. London, Ser. A, 151*, 455–464, 1935c.

Taylor, G. I., Statistical theory of turbulence, part IV, Diffusion in a turbulent air stream, *Proc. R. Soc. London, Ser. A, 151*, 465–478, 1935d.

Tennekes, H., Free convection in the turbulent Ekman layer of the atmosphere, *J. Atmos. Sci., 27*, 1027–1034, 1970.

Tennekes, H., Turbulent flow in two and three dimensions, *Bull. Am. Meteorol. Soc., 59*, 22–28, 1978.

Tennekes, H., and J. L. Lumley, *A First Course in Turbulence*, 300 pp., MIT Press, Cambridge, Mass., 1972.

Venkatram, A., and J. C. Wyngaard, Eds., *Lectures on Air Pollution Modeling*, 390 pp., Am. Meteorol. Soc., Boston, Mass., 1988.

Webb, E. K., Temperature and humidity structure in the lower atmosphere, in *Geodetic Refraction: Effects of Electromagnetic Wave Propagation Through the Atmosphere*, edited by F. K. Brunner, pp. 85–141, Springer-Verlag, New York, 1984.

Wesely, M. L., The combined effect of temperature and humidity fluctuations on refractive index, *J. Appl. Meteorol., 15*, 43–49, 1976. (Reproduced in *Turbulence in a*

Refractive Medium, edited by E. L. Andreas, *SPIE Milestone Ser., MS 25*, 231–237, 1990.)

Willis, G. E., and J. W. Deardorff, A laboratory model of the unstable planetary boundary layer, *J. Atmos. Sci., 31*, 1297–1307, 1974.

Wyngaard, J. C., On surface-layer turbulence, in *Workshop on Micrometeorology*, edited by D. A. Haugen, 392 pp., Am. Meteorol. Soc., Boston, Mass., 1973.

Wyngaard, J. C., Atmospheric turbulence, *Annu. Rev. Fluid Mech., 24*, 205–233, 1992.

Wyngaard, J. C., and B. Kosovic, Similarity of structure-function parameters in the stably stratified boundary layer, *Boundary Layer Meteorol., 71*, 277–296, 1994.

Wyngaard, J. C., and M. A. LeMone, Behavior of the refractive index structure parameter in the entraining convective boundary layer, *J. Atmos. Sci., 37*, 1573–1585, 1980. (Reproduced in *Turbulence in a Refractive Medium*, edited by E. L. Andreas, *SPIE Milestone Ser., MS 25*, 383–395, 1990.)

Wyngaard, J. C., O. R. Coté, and Y. Izumi, Local free convection, similarity, and the budgets of shear stress and heat flux, *J. Atmos. Sci., 28*, 1171–1182, 1971a.

Wyngaard, J. C., Y. Izumi, and S. A. Collins Jr., Behavior of the refractive index structure parameter near the ground, *J. Opt. Soc. Am., 61*, 1646–1650, 1971b. (Reproduced in *Turbulence in a Refractive Medium*, edited by E. L. Andreas, *SPIE Milestone Ser., MS 25*, 322–326, 1990.)

Wyngaard, J. C., W. T. Pennell, D. H. Lenschow, and M. A. LeMone, The temperature-humidity covariance budget in the convective boundary layer, *J. Atmos. Sci., 35*, 47–58, 1978. (Reproduced in *Turbulence in a Refractive Medium*, edited by E. L. Andreas, *SPIE Milestone Ser., MS 25*, 371–382, 1990.)

Zhang, D. L., H. R. Chang, N. L. Seaman, T. T. Warner, and J. M. Fritsch, A two-way interactive nesting procedure with variable terrain resolution, *Mon. Weather Rev., 114*, 1330–1339, 1986.

X. Di, Applied Research Laboratory, Pennsylvania State University, 204 Applied Science Building, University Park, PA 16802.

K. E. Gilbert, National Center for Physical Acoustics, University of Mississippi, 1 Coliseum Drive, University, MS 38677. (kgilbert@olemiss.edu)

S. J. Kimmel, M. Otte, N. Seaman, and J. C. Wyngaard, Department of Meteorology, College of Earth and Mineral Sciences, Pennsylvania State University, 503 Walker Building, University Park, PA 16802-5013. (jcw9@psu.edu)

(Received April 26, 2000; revised November 21, 2000; accepted December 12, 2000.)